The Journal of Neuroscience, June 15, 1999, *19*(12):4921–4937

$GABA_A$ Receptor Subunit Composition and Functional Properties of Cl^- Channels with Differential Sensitivity to Zolpidem in Embryonic Rat Hippocampal Cells

Dragan Maric,[1] Irina Maric,[1] Xiling Wen,[1] Jean-Marc Fritschy,[2] Werner Sieghart,[3] Jeffery L. Barker,[1] and Ruggero Serafini[1]

[1]*Laboratory of Neurophysiology, National Institute of Neurological Disorders and Stroke, National Institutes of Health, Bethesda, Maryland 20892,* [2]*Institute of Pharmacology, University of Zurich, CH-8057 Zurich, Switzerland, and* [3]*Department of Biochemical Psychiatry, University Clinic for Psychiatry, A-1090 Vienna, Austria*

Using flow cytometry in conjunction with a voltage-sensitive fluorescent indicator dye (oxonol), we have identified and separated embryonic hippocampal cells according to the sensitivity of their functionally expressed $GABA_A$ receptors to zolpidem. Immunocytochemical and RT-PCR analysis of sorted zolpidem-sensitive (ZS) and zolpidem-insensitive (ZI) subpopulations identified ZS cells as postmitotic, differentiating neurons expressing $\alpha2$, $\alpha4$, $\alpha5$, $\beta1$, $\beta2$, $\beta3$, $\gamma1$, $\gamma2$, and $\gamma3$ $GABA_A$ receptor subunits, whereas the ZI cells were neuroepithelial cells or newly postmitotic neurons, expressing predominantly $\alpha4$, $\alpha5$, $\beta1$, and $\gamma2$ subunits. Fluctuation analyses of macroscopic Cl^- currents evoked by GABA revealed three kinetic components of $GABA_A$ receptor/Cl^- channel activity in both subpopulations. We focused our study on ZI cells, which exhibited a limited number of subunits and functional channels, to directly correlate subunit composition with channel properties. Biophysical analyses of GABA-activated Cl^- currents in ZI cells revealed two types of receptor-coupled channel properties: one comprising short-lasting openings, high affinity for GABA, and low sensitivity to diazepam, and the other with long-lasting openings, low affinity for GABA, and high sensitivity to diazepam. Both types of channel activity were found in the same cell. Channel kinetics were well modeled by fitting dwell time distributions to biliganded activation and included two open and five closed states. We propose that short- and long-lasting openings correspond to $GABA_A$ receptor/Cl^- channels containing $\alpha4\beta1\gamma2$ and $\alpha5\beta1\gamma2$ subunits, respectively.

Key words: $GABA_A$ receptors; zolpidem; oxonol; FACS; development; rat; hippocampus

Zolpidem is an imidazopyridine hypnotic sedative that is thought to produce its effects by interaction with the benzodiazepine binding site on $GABA_A$ receptor/Cl^- channels (for review, see Sanger et al., 1994). Zolpidem binds to benzodiazepine sites on the receptor–channel complex with an affinity that depends on α subunit composition (Ruano et al., 1992). In the adult rat brain, three zolpidem binding sites have been correlated with $GABA_A$ receptor subunit expression: a high-affinity site (K_d, 10–20 nM) on $\alpha1$-containing receptors, a low-affinity site (K_d, 200–300 nM) on $\alpha2$- and $\alpha3$-containing receptors, and a very-low-affinity site (K_d, 4-l0 μM) on $\alpha5$-containing receptors (McKernan et al., 1991; Ruano et al., 1992; Mertens et al., 1993).

During embryonic development, $GABA_A$ receptor subunits emerge throughout the rat CNS, with elevated expressions of $\alpha2$, $\alpha3$, $\alpha4$, and $\alpha5$ subunit transcripts but quite low levels of the $\alpha1$ subunit mRNA (Laurie et al., 1992; Poulter et al., 1992). The emergence of the $\alpha1$-containing $GABA_A$ receptors during the early postnatal period parallels the appearance of fast inhibitory GABAergic transients in hippocampal and cortical regions, whereas the abundance of other α subunits before birth is presumed to be involved in morphogenic events. However, the subunit composition and the functional properties of $GABA_A$ receptors expressed during embryogenesis remain largely unexplored. Ma and Barker (1995) have proposed that $\alpha4$, $\beta1$, and $\gamma1$ are among the earliest expressed subunits, with their transcripts emerging among neuroepithelial cells. $\alpha3$, $\beta3$, and $\gamma2$ subunit transcripts and proteins have been reported in differentiating neurons of the cortical plate region (Maric et al., 1997). Unitary properties of $GABA_A$ receptor/Cl^- channels have been investigated in several areas of the developing brain, and differential localization of the $\alpha2$ and $\alpha3$ subunit mRNA has been correlated to different channel kinetics in these areas (Serafini et al., 1998a).

Here, we have used zolpidem to correlate subunit composition with the properties of native $GABA_A$ receptor/Cl^- channels expressed by embryonic hippocampal cells. First, we isolated subpopulations of cells whose functional $GABA_A$ receptors exhibited differential sensitivity to zolpidem using a potentiometric dye and a fluorescence-activated cell sorter (FACS). Sorted cells were then characterized for their neuronal epitope and $GABA_A$ receptor subunit expressions. Finally, biophysical properties of $GABA_A$ receptors/Cl^- channels in sorted cells were inferred using fluctuation analysis of macroscopic currents or measured directly with single-channel recordings. We focused our study on zolpidem-insensitive cells, which were newly postmitotic neurons that expressed $\alpha4$, $\alpha5$, $\beta1$, and $\gamma2$ subunits. Channel properties of these cells were correlated with sensitivity to diazepam and affinity for GABA. Probable subunit compositions of native receptors were inferred by correlating the observed properties with those of recombinant receptors expressing known subunit con-

Received Dec. 4, 1998; revised April 1, 1999; accepted April 6, 1999.

Correspondence should be addressed to Dr. D. Maric, Laboratory of Neurophysiology, National Institute of Neurological Disorders and Stroke, National Institutes of Health, Building 36, Room 2C-02, Bethesda, MD 20892.

Dr. Serafini's present address: Department of Anesthesiology Research Unit, Washington University School of Medicine, St. Louis, MO 63110.

structs. The results imply that short-lasting channels may be composed of $\alpha4\beta1\gamma2$ subunits, whereas long-lasting channels may include $\alpha5\beta1\gamma2$ subunits.

A preliminary report of this work has been presented in abstract form (Serafini et al., 1996).

MATERIALS AND METHODS

Cell dissociation

Timed pregnant embryonic day 19 (E19) Sprague Dawley rats (Taconic Farms, Germantown, NY) were killed by CO_2-induced anoxia. Embryos were placed in PBS, and a standard atlas (Paxinos et al., 1991) was used to determine the embryonic age by measuring the crown–rump length. Hippocampi were dissected out and incubated for 45 min at 37°C in Earle's balanced salt solution containing 20 U/ml papain (Boehringer Mannheim, Indianapolis, IN), 0.01% DNase (Boehringer Mannheim), and 0.5 mM EDTA (Sigma, St. Louis, MO). After gentle trituration, the single-cell suspension was washed three times in a physiological medium (medium A; in mM: 145 NaCl, 5 KCl, 1.8 $CaCl_2$, 0.8 mM $MgCl_2$, 10 HEPES, pH 7.3, and 10 glucose), supplemented with 1 mg/ml fatty acid-free bovine serum albumin (Sigma).

Fluorescence-activated cell analysis and sorting

At the beginning of an experiment, the cells were resuspended in a "low-Cl^-" medium A in which 145 mM NaCl was substituted with an equimolar concentration of Na isethionate (Sigma). This reduced extracellular Cl^- to 20 mM, thereby enhancing the transmembrane Cl^- ion gradient and thus amplifying GABA-induced depolarizing responses by shifting the Cl^- ion equilibrium potential. Membrane potential changes were detected using bis-(1,3-dibutyl barbituric acid) trimethine oxonol (Molecular Probes, Eugene, OR), which equilibrates with the cell according to its transmembrane potential and reports potentiometric signals over an ~10-fold dynamic range (Maric et al., 1998). Oxonol fluorescence (FL_{OX}) intensity was measured using the FACSTAR$^+$ flow cytometer (Becton Dickinson, Mountain View, CA). Cells were excited using an argon ion laser (model 2016; Spectra Physics, Mountain View, CA) operated at 500 mW and tuned to 488 nm, whereas the FL_{OX} emission was detected with a bandpass filter set at 530 ± 30 nm. All experiments were performed at room temperature. The cell suspensions were stained with 200 nM oxonol for 2 min, and baseline FL_{OX} was recorded in 10,000 cells at 2000 cells/sec. The cells were then stimulated with 1–10 μM GABA, with and without 25 nM–10 μM zolpidem, and the resulting FL_{OX} signals were profiled after 2 min. FL_{OX} distributions were quantified and illustrated as single-parameter frequency histograms using the Cell Quest data acquisition and analysis software (Becton Dickinson), with which modes, coefficients of variation, and peak amplitudes could be calculated. FL_{OX} profiles under control and experimental conditions were analyzed either by integration of the area under each peak or by measuring the relative amplitudes of their respective modes or with cumulative histogram statistics (Kolmorogov–Smirnov), all of which gave comparable results. Overlays of the control and experimental FL_{OX} histograms permitted quantitative analysis of the potentiometric response. The modal values of FL_{OX} distributions were calibrated in terms of estimated membrane potential (Maric et al., 1998). Cells without detectable zolpidem-modulated responses to GABA were sorted from cells whose GABAergic depolarization was intensely potentiated by zolpidem using the electronic gates shown in Figure 1C. Sorted cells were then washed, restained with oxonol, restimulated with GABA and zolpidem, and reanalyzed to test for sort fidelity, which was always ≥95% (Fig. 2). After sorting, the viability of the cells remained unchanged, with <5% trypan blue- or propidium iodide-positive (dead) cells in each sorted subpopulation.

Immunocytochemistry

Sorted cells were plated on poly-D-lysine (Sigma)-coated eight-well glass microscope slides (Nalge Nunck International, Naperville, IL) for 2 hr at 37°C and then fixed in 4% paraformaldehyde (Polysciences, Warrington, PA) for 15 min at room temperature. The developmental expression of antigens characteristic of precursor cells and differentiating neurons was enumerated by immunoreacting cells with the following antibodies: rabbit anti-nestin (a gift from R. McKay, National Institutes of Health, Bethesda, MD), a mixture of tetanus toxin fragment C (TnTx) and mouse anti-TnTx (Boehringer Mannheim), and mouse anti-class III β-tubulin (TuJ-1; Babco, Richmond, CA). Cells were immunoreacted with a mixture of 4 μg/ml TnTx and anti-TnTx (1:2000) or double-immunoreacted with anti-nestin (1:1000) and TuJ-1 (1:5000) antibodies for 1 hr at room temperature. The immunoreacted epitopes were then visualized by incubating the cells with appropriate secondary antibodies conjugated with FITC or rhodamine (Jackson ImmunoResearch, West Grove, PA). The percent of immunopositive cells was quantified by counting ~400 cells in four fields using standard fluorescence microscopy (Axiophot; Carl Zeiss, Thornwood, NY).

The expression of 11 $GABA_A$ receptor subunits in the sorted cells was investigated using specific antibodies generated against the peptide sequences depicted in parentheses: guinea pig polyclonal antibodies specific for α2 (1–9 residues) and α3 (1–15 residues) subunits (generated by J.-M.F.) and rabbit polyclonal antibodies specific for α1 (1–9 residues), α4 (379–421 residues), α5 (2–10 residues), β1 (350–404 residues), β2 (351–405 residues), β3 (345–408 residues), γ1 (324–366 residues), γ2 (319–366 residues), and γ3 (322–372 residues) subunits (generated by W.S.). The characterization and specificity of these antibodies have been described in detail elsewhere (Benke et al., 1991, 1997; Buchstaller et al., 1991; Marksitzer et al., 1993; Mertens et al., 1993; Mossier et al., 1994; Todd et al., 1996; Sperk et al., 1997). The cells were immunoreacted with guinea pig antibodies diluted 1:1000 or rabbit antibodies diluted 1:100–300 overnight at room temperature. In control slides, the primary antibodies were substituted with diluent only. Biotinylated donkey antibodies against appropriate species (Jackson ImmunoResearch) were used as secondary reagents. All antibodies were diluted in PBS containing 10% normal rat serum and 10% normal donkey serum to prevent nonspecific binding. Finally, the cells were reacted with streptavidin-conjugated horseradish peroxidase (Jackson ImmunoResearch) and developed in 3-amino-9-ethyl carbazole (AEC) substrate [25 mg of AEC (Sigma) in 100 ml of acetate buffer] with 0.01% H_2O_2 for 10–15 min at room temperature. After the slides were coverslipped, ~400 cells in four fields were imaged using a transmission light microscope connected to the Macintosh workstation. The percentage of immunopositive cells in each field was counted using the thresholding function of the NIH Image software.

In some experiments, E19 rat brains were fixed in 4% paraformaldehyde for 4 hr, cryoprotected in 30% sucrose for several days, and frozen in liquid nitrogen-cooled isopentane. Twenty-micrometer-thick coronal sections were cut using a cryostat, dried at room temperature for 1 hr, and immunostained with different $GABA_A$ receptor subunit-specific antibodies as described above.

PCR amplification of transcripts for $GABA_A$ receptor subunits

A previously established reverse transcription (RT)-PCR protocol (Somogyi et al., 1995) was used to measure $GABA_A$ receptor subunit gene expression in sorted cells. Gene-specific primers were designed from GenBank sequences using the Oligo software (National Biosciences, Plymouth, MN) as described (Ma et al., 1993). Total RNA was isolated from 2×10^6 sorted cells using RNAstat 60 (Tel-Test, Friendswood, TX) and the protocol recommended by the manufacturer. To confirm the purity of the product RNA, absorbtion ratios at 260:280 nm were determined to be >1.8 for all samples. RT and PCR were performed in a Perkin-Elmer 9600 thermal cycler using the Perkin-Elmer GeneAmp RNA PCR kit (Perkin-Elmer, Norwalk, CT). Two hundred nanograms of total RNA were used for each 100 μl PCR reaction. The PCR reaction was initiated using a hot start at 90°C to avoid mispriming. The thermal cycling protocol included a 90 sec preincubation at 97°C, followed by 35 cycles of 30 sec at 95°C (dissociation), 45 sec at 60°C (primer annealing), and 60 sec at 72°C (extension). Amplification was within the exponential range. PCR product identities were confirmed by restriction enzyme digestion. All RT and PCR reactions contained control RNA (transcribed from PAW 108 plasmid DNA; Applied Biosystems, Foster City, CA) to eliminate inefficient reactions from the analysis. PCR products were separated on 15-well 8–16% polyacrylamide gradient gels (Novex, San Diego, CA), using BioMarker low-DNA size standards (Bio Ventures, Murfreesboro, TN) as a reference. Gels were stained for 30 min with 0.1% ethidium bromide solution, illuminated on a UV transilluminator, and documented with black-and-white instant film.

Electrophysiology

Solutions and recordings. Extracellular solution contained (in mM): 140 NaCl, 5 KCl, 2 $CaCl_2$, 1 $MgCl_2$, 10 glucose, and 10 HEPES-NaOH. Intracellular pipette solution for whole-cell recording contained (in mM): 145 CsCl, 2 $MgCl_2$, 1.1 EGTA, 0.1 $CaCl_2$, 10 HEPES-CsOH, and 5

MgATP. Osmolarity and pH of all solutions were adjusted to 300–320 mOsm/kg and 7.2–7.3, respectively. Sorted cells were plated on plastic 35 mm dishes for 1 hr at 37°C in the extracellular medium. Pipettes made of thin glass with filament (WPI, Sarasota, FL) were pulled by a computerized BB-CH-PC puller (Mecanex, Geneva, Switzerland). Whole-cell patch-clamp recordings were performed at room temperature. Series resistance was <20 MΩ and was 50–80% compensated. Pipette currents were monitored via a Ag-AgCl wire and amplified through an Axopatch 200 amplifier (Axon Instruments, Foster City, CA) in the resistive head stage mode, displayed on a chart recorder, and recorded on tape for off-line analysis. Drugs were applied to the cells via low-level pressure from closely positioned micropipettes. Stock solutions of 1 mM were diluted with extracellular medium to obtain final drug concentrations used in the experiments.

Quantitative analysis of GABA-activated Cl^- currents and channels. Membrane currents were recorded at a low gain as a DC signal and then amplified, filtered, and stored on tape. For the analysis, data were played back, high-pass-filtered at 0.1 Hz through a homemade filter, low-pass-filtered at 1 kHz through an 8-pole Butterworth filter (901 Frequency Devices, Haverhill, MA), and digitized at 2 kHz through a National Instruments (Austin, TX) LAB PC acquisition board. Data were analyzed by Strathclyde Electrophysiological Software (University of Strathclyde, Glasgow, Scotland). Spectral analysis of GABA-evoked Cl^- currents was performed as previously reported (Serafini et al., 1995, 1998a,b). We have facilitated the study of native channel properties by FACS-sorting subpopulations of embryonic hippocampal cells with minimal numbers of $GABA_A$ receptor/Cl^- channels and then using algorithms to analyze openings, which control for bandwidth limitations and multiple superimposed channels. The low numbers of channels together with low levels of baseline noise allowed recordings of single-channel activities at wide bandwidth (0.5–1 kHz).

Quantitative analysis was performed in two different ways. First, we have selected stretches of recording from each cell containing only a few superimposed events and performed analysis of dwell time distributions as previously reported (Kristiansen et al., 1995; Serafini et al., 1995). Dwell time distributions were also analyzed through algorithms derived for recordings with multiple superimposed events (Kijima and Kijima, 1987) and with bandwidth limitations (Hawkes et al., 1992).

The following equations were derived by Kijima and Kijima (1987) to study patch recordings with multiple channels. The distribution function of dwell time of m open channels on a membrane with N number of total channels is $Z_{N,m}(t)$. The corresponding probability density function is $Y_{N,m}(t)$:

$$Z_{(N,m)}(t) = \frac{2\{1 - P_o(\infty)\}P_o(\infty)\partial_t(Z_{sop}^m Z_{ssh}^{N-m})}{\{m(1 - P_o(\infty)) + (N - m)P_o(\infty)\}\bar{f}_{tr}}$$

$$Y_{(N,m)}(t) = -\partial_t Z_{(N,m)}(t).$$

P_o is the steady-state open probability; ∂_t is the derivative of the function versus time; f_{tr} is the transition frequency; and $z_{ssh}(t)$ is the probability that the channel is in any of the shut states and is kept shut until time t. $z_{sop}(t)$ is the probability that the channel is in any of the open states and is kept open until time t. $z_{sop}(t)$ and $z_{ssh}(t)$ are calculated as follows:

$$z_{ssh}(t) = \sum_{I=1}^{L}\sum_{J=1}^{L}\frac{p_J{}^{(\infty)}q_{J,I}}{1 - P_o{}^{(\infty)}}$$

$$z_{sop}(t) = \sum_{I''=L+1}^{Q}\sum_{I'=L+1}^{Q}\frac{p_{I'}{}^{(\infty)}q_{I',I''}}{P_o{}^{(\infty)}}.$$

The shut states are $1, \ldots, L$. The open states are $L + 1, \ldots, Q$. The conditional probability $q_{I',I}(t)$ [or $q_{J,I}(t)$] is the probability that the channel that is in the open (or shut) state $S_{I'}$ (S_J) at $t = 0$ ends up in the open (or shut) state again $S_{I''}$ (S_I) at the time t without shutting (or opening) from $t = 0$ to time t. However, the actual $q_{I',I''}(t)$ used in our calculations is the corresponding value for a recording with interval omission attributable to bandwidth limitations [$^AR_i(t)$] (Hawkes et al., 1992) and is the probability that the channel starting in an open state at time 0 remains in an open state at time t, without any detected shut state between 0 and t. The following equations were derived by Hawkes et al. (1992). Briefly, using the same terminology as Hawkes et al. (1992):

$$^AR_{ij}(t) = P[X(t) = j \text{ and no shut time is detected over } (0, t)\,|\,X(0) = i]$$

$$W(s) = sI - H(s)$$

$$H(s) = Q_{AA} + Q_{AS}\left(\int_0^\tau e^{-st}e^{Qsst}dt\right)Q_{SA}$$

$$^AR_{ij}(t) \sim \sum_{l=1}^{k_A}\frac{e^{sit}c_i r_i W'(s_i)c_i}{r_j}.$$

where τ is the dead time of the system, c_i and r_i are the right and left eigenvectors of $H(s_i)$, corresponding to the root s_i, which is also an eigenvalue of $H(s_i)$. Q_{AA}, Q_{AS}, and Q_{SA} are the matrices of transition rates between open states, closed states, and open and closed states, respectively; $\exp(Q_{SS}t)$ has been calculated through spectral expansion, as indicated by Cohlqhoun and Hawkes (1977). To calculate the probability that a channel, being in the closed state at $t = 0$, apparently remains in the closed state at t, A and S were just inverted. Numerical calculations were performed using a program written by R. Serafini with Mathematica software (Wolfram, Champaigne, IL).

We have calculated the effects of activation of $GABA_A$ receptor/Cl^- channels on the cell membrane potential using Goldman–Hodgkin–Katz (GHK) equation:

$$E_{Rev} = \frac{RT}{F}\ln\left(\frac{P_{Cl}[Cl_i] + P_K[K_o] + P_{Na}[Na_o]}{P_{Cl}[Cl_o] + P_K[K_i] + P_{Na}[Na_i]}\right),$$

where E_{rev} is the reversal potential (or, in this case, the peak) of the membrane potential responses to GABA, P_{Na}, P_K, and P_{Cl} are Na, K, and Cl permeabilities, and R, T, and F have their usual meanings. We assumed that P_{Na} is very low, so that P_{Na} [Na] $\ll P_K$ [K] + P_{Cl} [Cl]. If $[K]_o$ = 5 mM, $[Cl]_o$ = 20 mM, and assuming that $[K]_i$ is ~140 mM (Maric et al., 1998) and $[Cl]_i$ is ~25 mM (Owens et al., 1996), then the GHK equation may be simplified to:

$$E_{Rev} = \frac{RT}{F}\ln\left(\frac{4P_{Cl} + P_K}{4P_{Cl} + 28P_K}\right).$$

The input resistance of embryonic cells recorded in the whole-cell mode is ~10 GΩ or more (Mienville et al., 1994). This would correspond, according to the constant field equation, to a permeability of 1.6×10^{-15} M. Based on these calculations, we estimated that the opening of even a single Cl^- ion channel with the unitary conductance characteristic for $GABA_A$ receptor/Cl^- channels quantified in these cells (see Figs. 7–9) would pass ~1 pA and depolarize an intact cell ~10 mV. The potentiometric measurements using flow cytometry have a resolution in the ~5–10 mV range (Maric et al., 1998). Therefore, even if the number of functionally expressed Cl^- channels was very low, the potentiometric recordings of intact cells make it likely that all the cells whose channels were activated by GABA and zolpidem could be detected.

In sum, the depolarizing shift induced in intact cells that have high input resistance will depend on the absolute number of channels whose gating is determined or enhanced by the ligand(s) and not on the relative fraction of channels that are sensitive to the modulator. Zolpidem-sensitive cells, expressing a large number of zolpidem-sensitive receptor/channels, might also express large numbers of receptor/channels that are insensitive to the ligand. In fact, the fraction of zolpidem-sensitive constructs may not necessarily be high in zolpidem-sensitive cells. Because the opening of individual channels may provide enough current to depolarize cells, zolpidem-insensitive cells should be truly deprived of zolpidem-sensitive receptor/channels. The zolpidem-insensitive population should therefore be composed of (1) cells with no GABA-evoked response, (2) cells with truly zolpidem-insensitive responses, and (3) cells with zolpidem-sensitive receptor/channels at very low density and/or very low P_{open} of each individual channel and/or a low unitary conductance, which together are insufficient to depolarize cells.

Experimental observations are mostly in agreement with these predictions (see Results). There was a marked potentiation by zolpidem of the GABA-evoked current in the zolpidem-sensitive cells. However, RT-PCR of subunit transcripts and subunit immunoreactivity revealed the presence of high levels of α5 subunits in the zolpidem-sensitive popula-

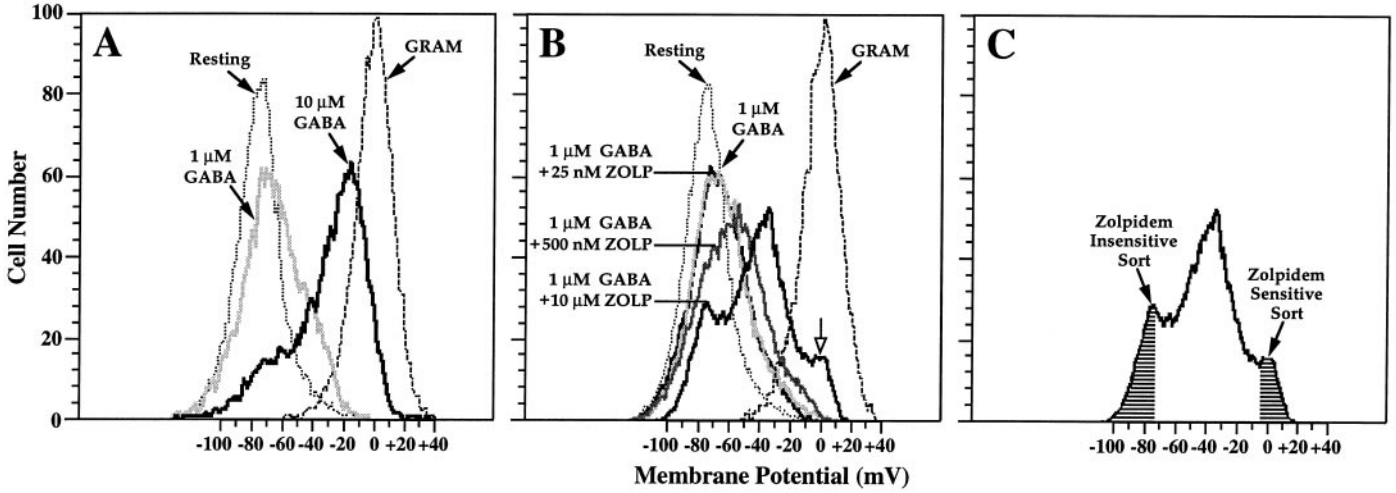

Figure 1. Zolpidem potentiates GABA-induced depolarization in many embryonic hippocampal cells. Data are frequency histograms of the oxonol fluorescence (FL_{OX}) intensity distribution of 10,000 cells compiled in 5 sec using flow cytometry. Potentiometric profiles of FL_{OX} were acquired under resting conditions and at the peak of the response after exposure to GABA, with and without different concentrations of zolpidem (*ZOLP*). Gramicidin (*GRAM*) was added afterward to reveal the FL_{OX} distribution equivalent to 0 mV. *A*, Within 2 min of stimulation, 1 μM GABA induces a modest depolarization in 25–30% of the cells, whereas 10 μM GABA depolarizes ~85% of the cells, with a well defined FL_{OX} mode corresponding to −20 mV. *B*, Inclusion of 25 nM zolpidem with 1 μM GABA does not alter the cells depolarized by GABA, whereas additions of 500 nm and 10 μM zolpidem depolarize ~52 and ~67% of the cells, respectively, with ~20% of maximally potentiated cells depolarizing to ~0 mV (*open arrow*). *C*, The FL_{OX} distribution of cells in the presence of 1 μM GABA and 10 μM zolpidem is displayed to illustrate the sorting gates (*shaded areas*) used to separate cells without zolpidem modulation (*Zolpidem Insensitive Sort*) from cells with maximal zolpidem potentiation (*Zolpidem Sensitive Sort*).

tion, implying the coexistence of both zolpidem-sensitive and -insensitive constructs on these cells. The zolpidem-insensitive cells indeed corresponded to cells exhibiting voltage-clamp responses with no sensitivity to zolpidem. In agreement with theoretical considerations, we also found that not all cells were responding to GABA. However, we did not find evidence for cells expressing zolpidem-sensitive channels with low P_{open} and low conductance.

RESULTS

Zolpidem-sensitive and zolpidem-insensitive $GABA_A$ receptor Cl^- ion channels are expressed by embryonic hippocampal cells

GABA depolarized hippocampal cells in a dose-dependent manner over 1–10 μM, with 10 μM GABA depolarizing ~85% of the cells close to −20 mV from a resting potential of approximately −75 mV (Fig. 1*A*). One micromolar GABA induced modest but detectable depolarization (~10 mV) in ~25% of the cells. Zolpidem was added to 1 μM GABA to test for potentiating effects. Twenty-five nanomolar zolpidem had no effect, whereas 500 nM depolarized ~52% and 10 μM depolarized 67% of the cells, with 20% depolarizing close to 0 mV (Fig. 1*B*). Higher zolpidem concentrations had no further effects (data not shown).

Cells whose depolarizing responses to GABA were insensitive to 10 μM zolpidem and cells with GABA-induced depolarizations to ~0 mV in zolpidem were physically sorted with the FACSTAR$^+$ flow cytometer using the electronic gates shown in Figure 1*C*. GABA-induced depolarizations of sorted zolpidem-insensitive cells were not affected by 10 μM zolpidem (Fig. 2*A*). All sorted zolpidem-sensitive cells exhibited GABA-induced depolarizations that were potentiated by zolpidem (Fig. 2*B*), testifying to the high fidelity of the sort. Because the zolpidem-insensitive population also contained cells without depolarizing responses to 1 μM GABA, we added 10 μM GABA to discover the size of the population expressing functional $GABA_A$ receptors and found that ~60% responded (Fig. 2*C*). As expected, >97% of the cells in the zolpidem-sensitive subpopulation depolarized to 10 μM GABA (Fig. 2*D*). Depolarizing responses to GABA in both sorted subpopulations were Cl^- ion-dependent and completely blocked by preincubation of cells with 50 μM bicuculline (data not shown), identifying the involvement of functional $GABA_A$ receptor/Cl^- channels in both cell types.

Zolpidem-sensitive cells are differentiating neurons, whereas zolpidem-insensitive cells are undifferentiated, immature cells

Sorted cells were immunostained for specific epitopes. Nestin, an intermediate filament protein of neuroepithelium-derived progenitor cells (Hockfield and McKay, 1985), labeled 75% of the zolpidem-insensitive cells and only 3% of the zolpidem-sensitive cells (Fig. 3*A*). TnTx, a marker of postmitotic, differentiating embryonic neurons (Koulakoff et al., 1983; Maric et al., 1997), labeled only 5% of the zolpidem-insensitive cells and ~90% of the zolpidem-sensitive cells. Thus, the zolpidem-insensitive population was almost entirely composed of relatively immature, undifferentiated cells, whereas the great majority of zolpidem-sensitive cells were differentiating neurons. Immunostaining with the TuJ-1 antibody, which reacts with neuron-specific tubulin β III cytoskeletal protein (Lee et al., 1990; Menezes and Luskin, 1994), confirmed the neuronal phenotype of zolpidem-sensitive cells, because >90% of these cells were TuJ-1-positive. However, ~35% of the zolpidem-insensitive cells were also TuJ-1$^+$, indicating the presence of newly committed neurons in this subpopulation. Double labeling with anti-nestin and anti-TuJ-1 antibodies demonstrated many double-positive cells in the zolpidem-insensitive subpopulation (Fig. 3*B*), consistent with the relative immaturity of zolpidem-insensitive TuJ-1$^+$ neurons. In contrast, TuJ-1$^+$ neurons in the zolpidem-sensitive population were almost all nestin$^-$, characteristic of a more mature stage in neuronal differentiation. Morphologically, zolpidem-sensitive cells were visibly larger in diameter, and most exhibited processes, whereas zolpidem-insensitive cells were mostly spherical and smaller in diameter with few or no processes (Fig. 3*B*). Some of the heavily

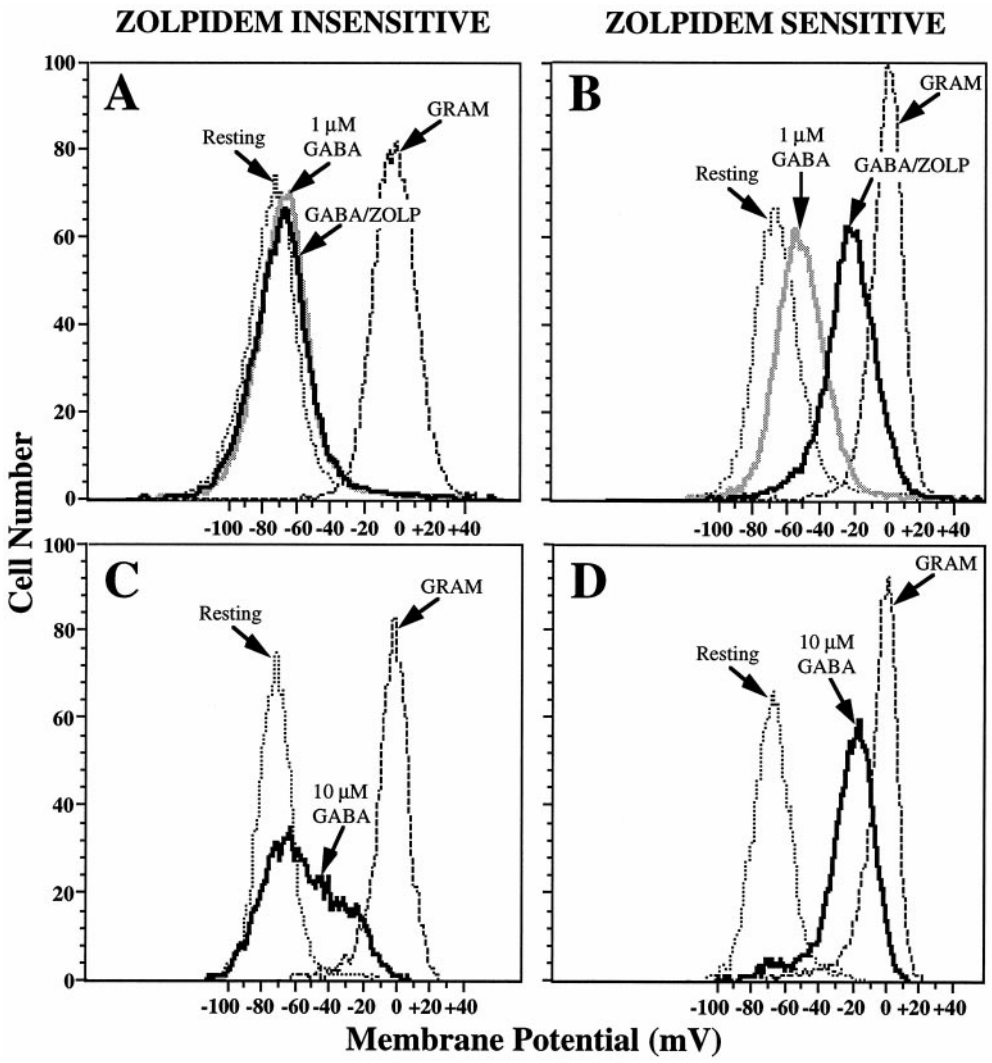

Figure 2. Reanalysis of zolpidem-sorted cells reveals high fidelity in the sorting. Potentiometry was performed as outlined in Figure 1. *A*, 1 μM GABA induces a just-detectable depolarization of zolpidem-insensitive cells that is not affected by 10 μM zolpidem (*ZOLP*). *B*, 1 μM GABA evokes a moderate depolarization of zolpidem-sensitive cells, all of which depolarize further in the presence of 10 μM zolpidem. *C*, 10 μM GABA depolarizes ~60% of the zolpidem-insensitive population. *D*, 10 μM GABA depolarizes >97% of the zolpidem-sensitive cells, with a well defined FL_{OX} mode corresponding to approximately −20 mV. *GRAM*, Gramicidin.

labeled TuJ-1 cells in the zolpidem-insensitive subpopulation exhibited processes, consistent with their neuronal lineage.

Contrasting $GABA_A$ receptor subunit expressions of zolpidem-sorted cells

The expressions of 11 different $GABA_A$ receptor subunits at protein and transcript levels in sorted cells were investigated using immunocytochemistry and RT-PCR. In the zolpidem-sensitive population, ~70–90% of cells immunostained with antibodies against the α4, α5, β1, β2, β3, γ2, and γ3 subunits (Fig. 4*A*). Approximately 40% of the cells were $\alpha 2^+$, and 25% were $\gamma 1^+$. The α3 subunit was expressed in <10%, whereas the α1 subunit was not detected. Thus, zolpidem-sensitive neurons expressed a wide variety of subunits, which may form different $GABA_A$ receptor constructs on the same cell.

In contrast, 40–50% of the cells in the zolpidem-insensitive population immunostained for α4, α5, β1, or γ2 subunits (Fig. 4*A*). The α2, β2, γ1, and γ3 subunits were present in ≤5% of the cells, whereas the α1, α3, and β3 subunits were virtually undetected. Because the potentiometric experiments (Fig. 2*C*) demonstrated that up to 60% of these cells were depolarized by GABA, most of these cells likely express or coexpress either α4β1γ2 and/or α5β1γ2 subunit constructs.

RT-PCR analysis revealed an abundance of subunit transcripts in zolpidem-sensitive cells with polyacrylamide gels showing high-intensity bands for α4, α5, β1, β2, β3, γ2, and γ3 (Fig. 4*B*), paralleling the subunit proteins most widely expressed (Fig. 4*A*). Low-intensity bands for α4, α5, β1, and γ2 were the most evident in the zolpidem-insensitive cells, corresponding to those proteins detected by immunocytochemistry. α1 subunit transcripts were detected only in the zolpidem-sensitive population, although α1 protein was not.

In immunocytochemical studies of intact hippocampal sections we verified the presence of the expressed subunit proteins (results to be published elsewhere). The α1 and α3 subunits were not detected, whereas the α2 and α3 subunits were present only in differentiating regions. All remaining subunits were detected in both proliferative and differentiating regions.

Cl^- currents evoked by GABA in sorted subpopulations differ in sensitivity to zolpidem and absolute density

We performed patch-clamp recordings of sorted cells within hours of plating to characterize $GABA_A$ receptor/Cl^- channel properties. GABA evoked inward current responses in all 22 zolpidem-sensitive neurons (Fig. 5*A*; $n = 5$ sorting experiments; mean ± SE of interexperiment variability, 92 ± 10%). The currents reversed polarity at the equilibrium potential for Cl^-,

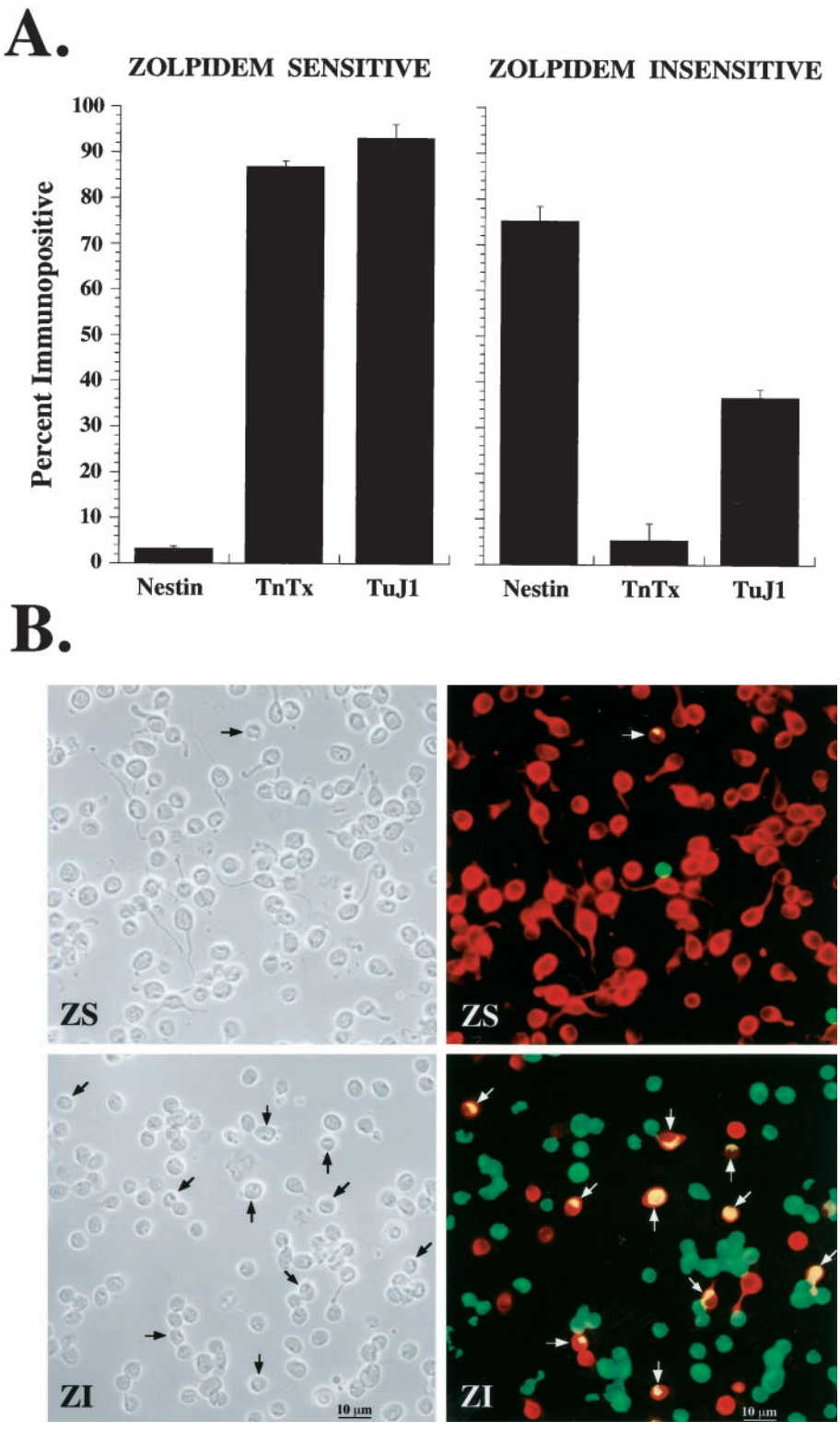

Figure 3. Zolpidem-sensitive cells are differentiating neurons, whereas the zolpidem-insensitive population mostly comprises immature cells. After sorting, zolpidem-sensitive and zolpidem-insensitive cells were plated and immunostained with antibodies against nestin, TnTx binding sites and TuJ-1. *A*, Virtually all of the zolpidem-sensitive cells are nestin$^-$, TnTx$^+$, and TuJ-1$^+$, whereas the zolpidem-insensitive cells are predominantly nestin$^+$ and TnTx$^-$, with a fraction (~35%) of them also expressing TuJ-1. *B*, Double immunostaining with anti-nestin (*green*) and TuJ-1 (*red*) antibodies demonstrates the abundance of double-positive young neurons (*yellow, arrows*) in the zolpidem-insensitive (*ZI*) but not in the zolpidem-sensitive (*ZS*) population. Data in *A* represent mean ± SE for three to five independent determinations.

which was ~0 mV (data not shown). The peak amplitude of the current response evoked by 2 μM GABA averaged 186 ± 49 pA ($n = 6$). Clear enhancement of the current response to GABA by 5–10 μM zolpidem was found in all six cells tested, without significant differences between the effects of 5 and 10 μM zolpidem (Fig. 5*A1*). Zolpidem potentiation of the GABA-evoked current response averaged 284 ± 52% of control. In zolpidem-insensitive cells, inward current responses to 2 μM GABA were highly variable in amplitude and decay, reversed at E_{Cl} (data not shown), and were detected in 115 of 143 cells tested (Fig. 5*B*; $n =$ 13 sorting experiments; mean ± SE of interexperiment variability, 85 ± 6%). The current response in some cells did not involve sufficiently sustained summation of channel openings to generate a steady current. Instead, unitary channel activity could be recorded in whole-cell mode at DC to ~1 kHz bandwidth (see below). When sustained, peak currents in zolpidem-insensitive

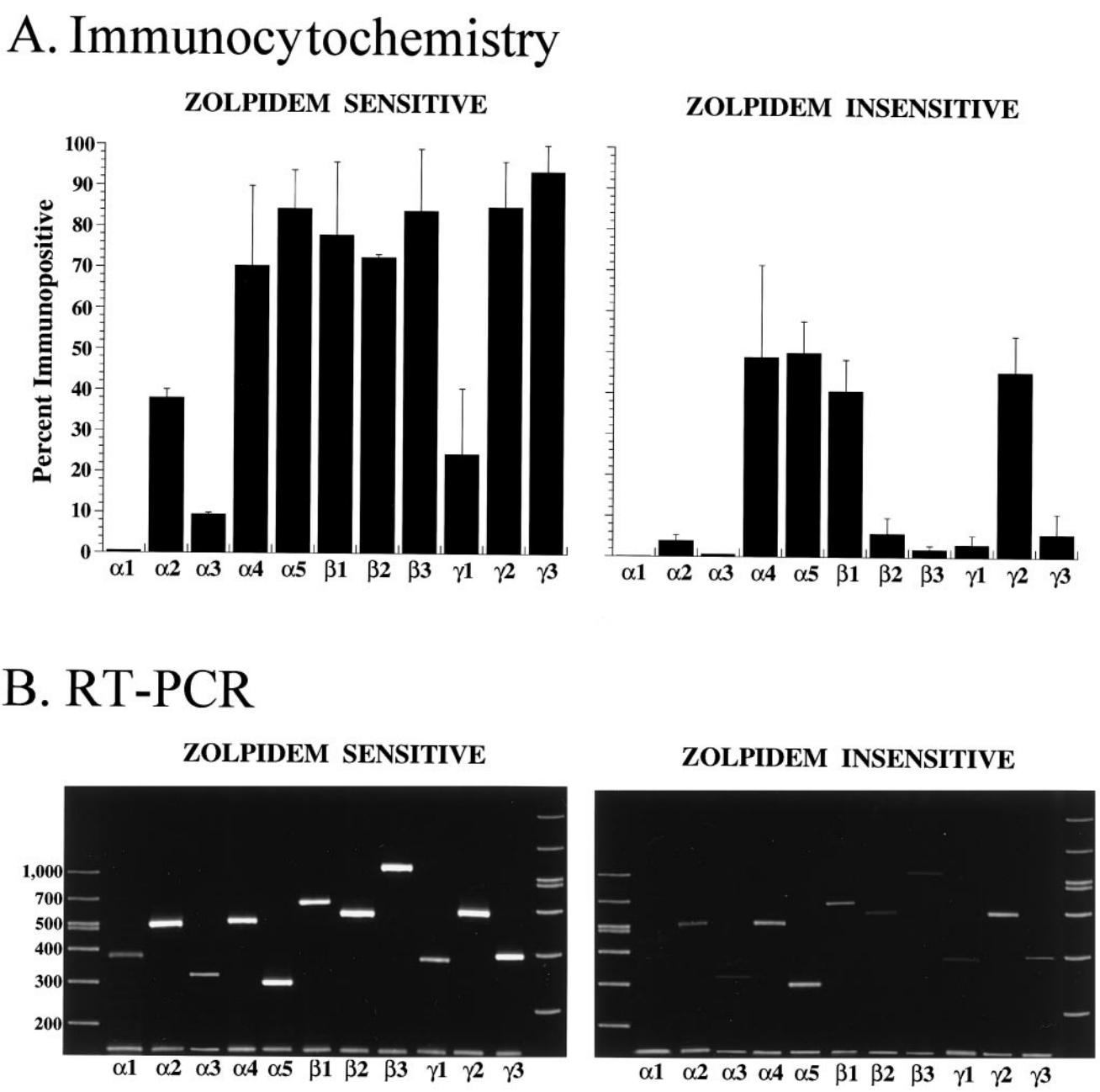

Figure 4. Immunocytochemical and RT-PCR analyses of 11 $GABA_A$ receptor subunits reveal different expression patterns in zolpidem-sensitive and zolpidem-insensitive populations. *A*, Eleven $GABA_A$ receptor subunit proteins in sorted populations were quantified immunocytochemically in terms of percent (mean ± SD) immunopositive cells. More than 70% of the zolpidem-sensitive cells immunostain for either $\alpha4$, $\alpha5$, $\beta1$, $\beta2$, $\beta3$, $\gamma2$, or $\gamma3$ subunits, whereas ~40% are $\alpha2^+$ and ~25% are $\gamma1^+$. Less than 10% are $\alpha3^+$, and none express $\alpha1$. In contrast, only four subunits are well expressed in the zolpidem-insensitive population: $\alpha4$, $\alpha5$, $\beta1$, and $\gamma2$. *B*, Ethidium bromide-stained polyacrylamide gels of RT-PCR products derived from the total RNA of the same number of zolpidem-sensitive and -insensitive cells are displayed together with the 149 bp product of amplified control RNA, which serves as an internal standard. The most intensely stained PCR products among zolpidem-sensitive cells correspond to the subunits expressed by the highest percentages of cells (see *A*). Fainter bands of other products parallel their more restricted cellular distributions. The $\alpha1$ transcript in zolpidem-sensitive cells can be detected in the absence of the protein. None of the bands derived from RT-PCR of zolpidem-insensitive cells is as intense as those found in analysis of zolpidem-sensitive cells, and the most intensely stained bands correspond to the four subunits, which are detected at the protein level in 40–50% of the cells. The $\alpha1$ transcripts are not detected in zolpidem-insensitive cells. Note that the bands of $\alpha1$–5 and $\beta1$ transcripts correspond to DNA size standards in the *left-most lane* of each panel, whereas the bands of $\beta2$, $\beta3$, and $\gamma1$–3 transcripts correspond to DNA size standards in the *right-most lane* of each panel.

cells averaged only 18.8 ± 4.8 pA (n = 74) and 36.5 ± 20.3 pA (n = 17) for responses evoked by 2 and 10 μM GABA, respectively. As expected, zolpidem (5–10 μM) had little, if any, detectable effects on the peak amplitudes of GABA-evoked responses (115 ± 9% of control) in these cells (Fig. 5*B*).

The ~10-fold greater amplitude of Cl^- currents evoked by 2 μM GABA in zolpidem-sensitive neurons could be related in part to differences in cell size. Capacitance values were used to index cell size. They averaged 4 ± 1 pF in four zolpidem-insensitive cells and 9 ± 2 pF in four zolpidem-sensitive neurons. Thus,

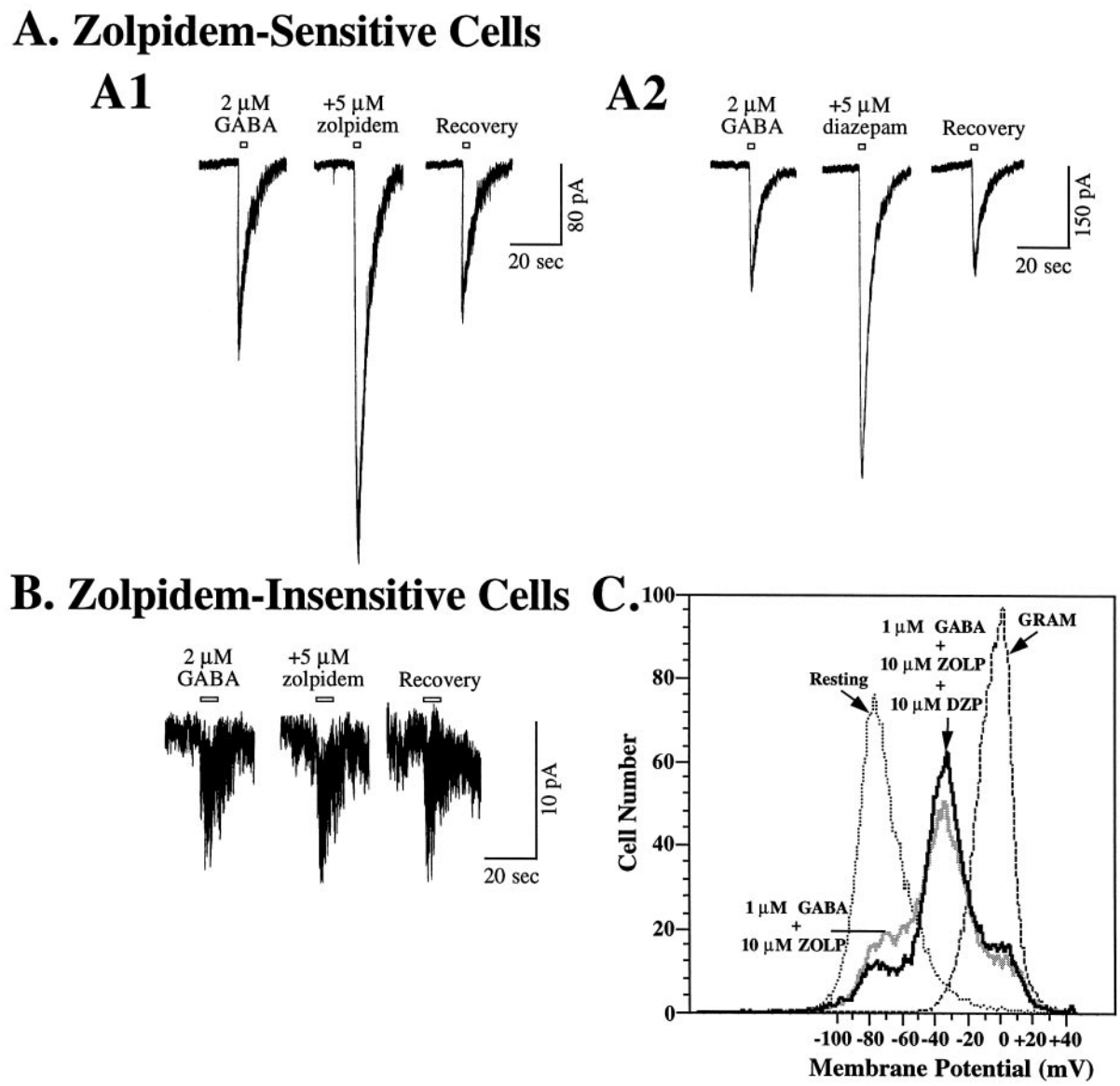

Figure 5. GABA-evoked Cl^- currents in sorted cells are differentially sensitive to zolpidem and diazepam. After sorting, cells were cultured for ~2 hr and then recorded in whole-cell mode and voltage-clamped at −60 mV before application of GABA, with and without zolpidem or diazepam. *A*, GABA evokes Cl^- currents of ~150 and ~170 pA in two different cells, which are reversibly potentiated approximately two-fold by zolpidem (*A1*) and by diazepam (*A2*). *B*, GABA evokes a low-amplitude current (<10 pA), which is not affected by zolpidem. *C*, FACS potentiometry reveals the presence of a subpopulation whose GABA-induced depolarization is zolpidem (*ZOLP*)-insensitive but is potentiated by diazepam (*DZP*), with some cells depolarizing to 0 mV, which is identified using gramicidin (*GRAM*).

zolpidem-sensitive neurons exhibited approximately twice the surface area, which is consistent with their larger cell diameters and the presence of processes. These results also demonstrate that zolpidem-sensitive neurons expressed a fivefold greater density of macroscopic GABA-activated Cl^- current.

Sorted subpopulations were also tested for their sensitivity to the benzodiazepine diazepam. Five micromolar diazepam potentiated responses to 2 μM GABA in three zolpidem-sensitive cells by 291 ± 42% (Fig. 5*A2*), mimicking the effects of zolpidem. Diazepam-induced potentiation was also present among zolpidem-insensitive cells, ranging from no effect to up to 300%. On average, the GABA-evoked current in diazepam-sensitive cells was increased to 212 ± 31% of control (n = 9 using 2 μM GABA; n = 2 using 10 μM GABA). Potentiometric measurements confirmed the presence of diazepam-modulated depolarizing responses to GABA among cells in the zolpidem-insensitive subpopulation (Fig. 5*C*). Thus, some zolpidem-insensitive cells exhibited $GABA_A$ receptor/Cl^- channels that were sensitive to diazepam.

Spectral analysis of Cl^- current responses evoked by GABA reveals complex channel kinetics

We used fluctuation analysis techniques to estimate the unitary properties of GABA-activated Cl^- channels underlying summated current responses. Three components of exponentially distributed activity accounted for all of the variance in the signals (summarized in Table 1). On average, there was detectably more (~62 vs 48%) contribution of the low-frequency (LF) component to current fluctuations induced by GABA on zolpidem-sensitive cells, which exhibited ~25% shorter time constants associated

Table 1. Elementary $GABA_A$ receptor/Cl^- channel properties and relative contributions estimated from spectral analyses of GABA-induced Cl^- currents in zolpidem-sensitive and zolpidem-insensitive cells

	τ_{LF}	A_{LF}	τ_{IF}	A_{IF}	t_{HF}	A_{HF}	γ	n
Zolpidem-sensitive	76 ± 7	62 ± 3	7 ± 1	22 ± 2	1.1 ± 0.1	16 ± 2	17 ± 1	8
Zolpidem-insensitive	99 ± 9	48 ± 1	6 ± 0.4	37 ± 5	0.7 ± 0.1	15 ± 1	19 ± 1	3

Data are mean ± SE of determinations carried out on n number of cells. τ_{LF}, τ_{IF}, and τ_{HF} are the time constants (in milliseconds) corresponding to the low-frequency (LF), intermediate-frequency (IF), and high-frequency (HF) components identified in spectral analyses of Cl^- current fluctuations induced by 2 μM GABA. A_{LF}, A_{IF}, and A_{HF} are the relative areas (contributions) of each component to the fluctuating signal. γ is the inferred unitary conductance in pS.

with this component. In contrast, there was considerably more contribution of intermediate-frequency (IF) activity (37 vs 22%) to GABA-induced currents evoked on zolpidem-insensitive cells, which exhibited a time constant similar to that inferred on zolpidem-sensitive cells. The residual, high-frequency (HF) contribution (~15% of the variance) was similar in both subpopulations, as was the estimated elementary conductance (~17–19 pS). More detailed analyses were performed on currents evoked by GABA in zolpidem-insensitive cells, because these cells only expressed α4, α5, β1, and γ2 subunits, thus increasing the possibility of correlating channel properties with subunit expression.

Heterogenous $GABA_A$ receptor/Cl^- channel properties in zolpidem-insensitive cells

There were no significant differences between estimated time constant or unitary conductance values for Cl^- channels underlying current responses evoked by 2 and 10 μM GABA in five cells (data not shown). On average, the LF component in spectral density plots accounted for ~50–60%, the IF activity accounted for ~20–30%, and the HF fluctuations accounted for the remaining ~10–20% of the total variance (Fig. 6*A3,B3,C3,D3*). Two distinctive sets of channel properties were quantified. The power density spectra of some cells were characterized by a relative abundance of power in the IF range (Fig. 6*A3,B3*), indicating the presence of one or more populations of exponentially distributed events with intermediate durations (~2–32 msec). The time constant of the LF component (τ_{LF}) ranged from 50 to 150 msec, whereas τ_{IF} values were 3–8 msec, and τ_{HF} estimates ranged over 0.2–0.6 msec. Cells with a pronounced contribution of the IF component (e.g., Fig. 6*A3,B3*) exhibited a relatively modest increase in current amplitude (40–200%) when 100 μM GABA was applied (Fig. 6*A1,A2*), whereas those with less IF but proportionally more LF activity (e.g., Fig. 6*C3,D3*) exhibited a dramatic ~7–8 fold increase in response to 100 μM GABA (Fig. 6*C1,C2*). The relative increase in current amplitude evoked by 100 μM GABA ($I_{100\ \mu M}/I_{10\ \mu M}$) correlated directly with the relative contribution of the LF component and inversely with that of the IF component (Table 2). Similarly, diazepam potentiation of GABA-evoked current correlated directly with the relative area of the LF component and inversely with the contribution of the IF component (Fig. 6*B1,B2,D1,D2*, Table 2).

These results reveal at least two distinct types of channel activity: one with a pronounced contribution of events intermediate in duration, which are nearly saturated at 10 μM GABA (EC_{50}, <10 μM) and relatively insensitive to diazepam; and the other with a prevalence of low-frequency (long-lasting) events (<5 Hz), an EC_{50} >10 μM, and an ~200% increase in amplitude promoted by diazepam.

Elementary properties of unitary $GABA_A$ receptor/Cl^- channels recorded whole-cell

GABA evoked single channel levels of activity in a subpopulation of zolpidem-insensitive cells (Fig. 7). Most of these recordings revealed approximately two to five channels having the same main conductance state (~26–30 pS). Kinetic analyses were performed on stretches with predominantly single-channel levels of activity. Open-time distributions of individual cells (derived from 180–6167 transitions) indicated at least two components (S, short; and L, long) with τ values of ~1 msec (τ_S) and 3–18 msec (τ_L), respectively (Fig. 7). In five of 12 cells exposed to 2 μM GABA, τ_L was <5 msec (4.7, 1.6, 2.0, 2.6, and 3.2 msec), whereas in four others τ_L was >7 msec (8.1, 10.1, 8.0, 7.3, and 7.4 msec), and in the remaining three τ_L exhibited intermediate values (6.7, 5.6, and 5.7 msec). In three cells exposed to 10 μM GABA, τ_L was >7 msec (9.7, 13.0, and 13.2 msec), whereas in the remaining three it was <7 msec (4.5, 3.0, and 3.9 msec). In two cells exposed to 20 μM GABA, τ_L was 4.9 and 4.7 msec. Arbitrarily, we have identified openings whose τ_L values were ≤5 msec as "fast channels" and those with τ_L of >7 msec as "slow channels."

Closed-time distributions (derived from 125–2076 events) could be fitted by three components with τ values of ~1, 5–10, and 30–400 msec (Fig. 7). A clear pattern of closed-time distributions was evident in cells exposed to 2 μM GABA. Fast channels exhibited τ_L values of <30 msec (14, 29.3, 7.7, 6.1, and 10.4 msec), whereas slow channels manifested exceptionally long τ_L values (138.1, 104, 38.7, 39.6, and 153.6 msec). However, when 10 μM GABA was used, these differences between fast and slow channels disappeared, and τ_L was always >87 msec.

We arbitrarily defined bursts of channel activity as groups of openings clustered by closures shorter than 10 msec. Clear differences in kinetics were recorded at 10 μM GABA, with fast channels exhibiting only short-lasting burst length durations (23.9, 20.4, and 22.7 msec) and slow channels only expressing long-lasting ones (75.1, 109, and 74.2 msec; Fig. 7). A few recordings suggested that both types of channel activity might be present on the same cell (data not shown). In contrast, no clear differences between the two types of channel activities were evident when 2 μM GABA was used; τ_L was always <25 msec. Although the time constants defined by the curve fitting and analysis are expected to be distorted by the presence of multiple channels, we resolved at least two distinct channel activities. Two channel activities were also detected from the cumulative probability distribution of the τ_L of the open times, which exhibited distinct plateaus at ~3 and ~9 msec (data not shown). Channels whose activity resulted in an open-time τ_L of 3 msec exhibited a burst length distribution with a long component (20–30 msec) together with a very high frequency of openings. The upper plateau of the probability distribution of the open-time τ_L indicated the presence of a second, distinct channel activity with markedly different properties.

Kinetic analyses of multiple slow and fast channel activities recorded at limited bandwidth

Because the groups of openings characterized by the cluster analysis were likely to correspond to distinct channel activities, we quantified their kinetics. For the fast channels, we analyzed

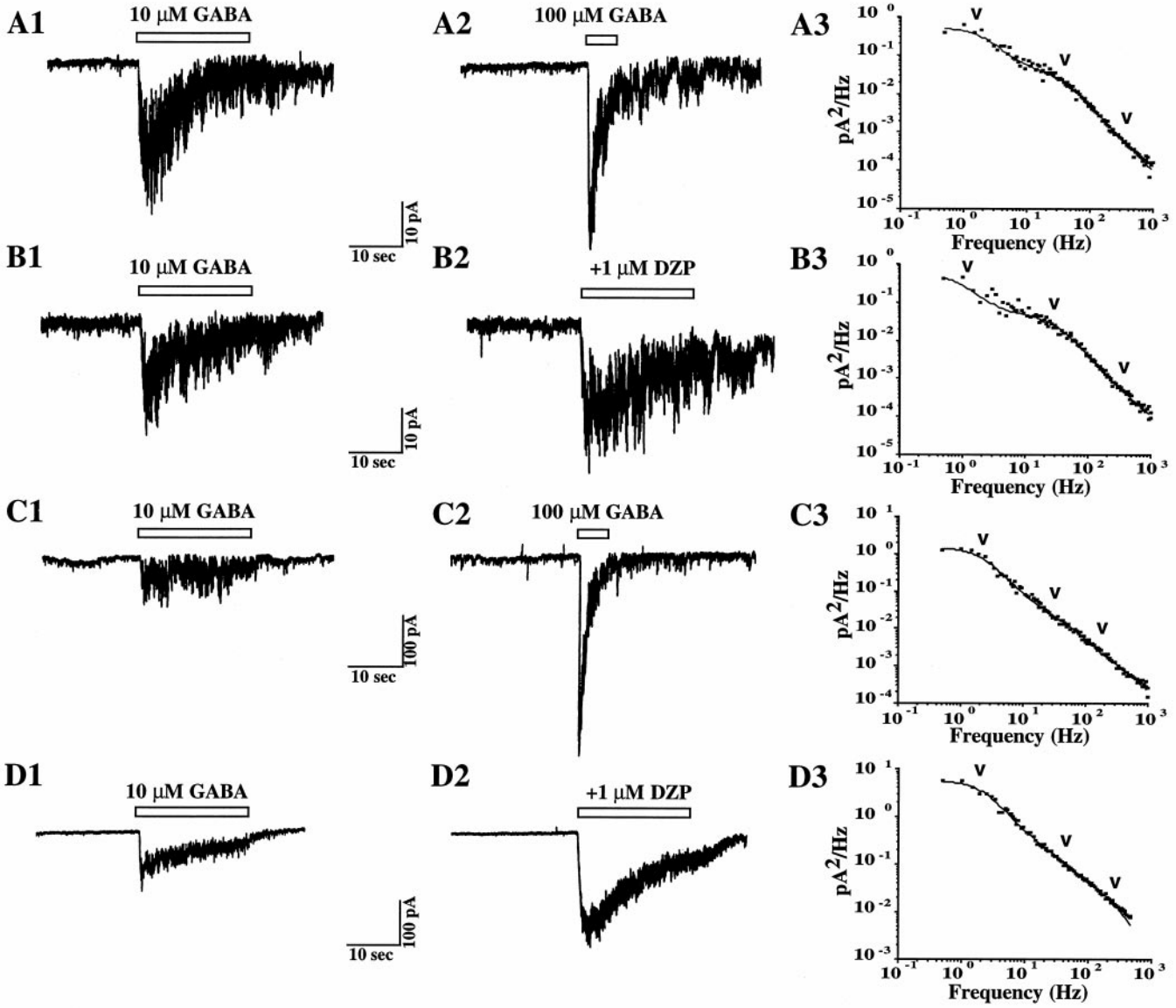

Figure 6. Heterogeneity of Cl^- current responses to GABA, with and without diazepam, and $GABA_A$ receptor/Cl^- channel properties among sorted zolpidem-insensitive cells. Four different cells in the zolpidem-insensitive population were clamped at −60 mV and then exposed to GABA, with and without diazepam (*DZP*). *A1, A2, B1, B2*, 10 μM GABA activates low-amplitude, fading currents (~20 pA) that are modestly enhanced in peak amplitude by 100 μM GABA (*A2*) or 1 μM DZP (*B2*). *C1, C2, D1, D2*, 10 μM GABA evokes larger-amplitude currents, which are more sustained and associated with dramatically more current enhancement when exposed to 100 μM GABA (*C2*) or 1 μM DZP (*D2*). *A3, B3, C3, D3*, Spectral density plots calculated for the fluctuations triggered by GABA in each cell show that power is exponentially distributed among three components whose corner frequencies (f_c) are identified with *downward arrowheads*. There is a relative abundance of power distributed in the IF range (*A3, B3*), which accounts for 50% of the variance, considerably more than in *C3* and *D3* (~30% contribution). Conversely, the LF component accounts for ~30% of the variance in *A3* and *B3* but ~70% in *C3* and *D3*. The f_c values indicate estimated τ_{LF} values of ~199 msec (*A3*), ~159 msec (*B3*), ~80 msec (*C3*), and ~72 msec (*D3*) and τ_{IF} values of ~4 msec (*A3*), 5.3 msec (*B3*), 3.9 msec (*C3*), and 3.7 msec (*D3*). The corresponding estimates for the high-frequency components are 0.2–0.5 msec.

Table 2. Dose-dependent increase and diazepam-induced potentiation of GABA-evoked Cl^- currents correlate with the relative contributions of different components rather than with estimated kinetics and conductance

	τ_{LF}	A_{LF}	τ_{IF}	A_{IF}	τ_{HF}	A_{HF}	γ	n
$I_{GABA\ 100/10\ \mu M}$	NS	**0.78**	NS	**0.84**	NS	NS	NS	7
		.04		.02				
Diazepam potentiation	NS	**0.77**	NS	**0.66**	NS	**0.51**	NS	18
		0.0003		0.0004		0.04		

Spectral analyses were performed on Cl^- currents (*I*) evoked in the same cell either by 10 and 100 μM GABA or by 10 μM GABA and then 10 μM GABA plus 10 μM diazepam. Only values for which $p < 0.05$ are enumerated. *R* values are in bold, *p* in regular font; NS, not significant; *n* = number of cells. Neither τ nor γ values correlate significantly with enhanced current amplitudes. Rather, current enhancement correlates highly and significantly with reciprocally changing contributions of the two dominant components (more LF, less IF). The contribution of high-frequency signals also decreases significantly with diazepam potentiation.

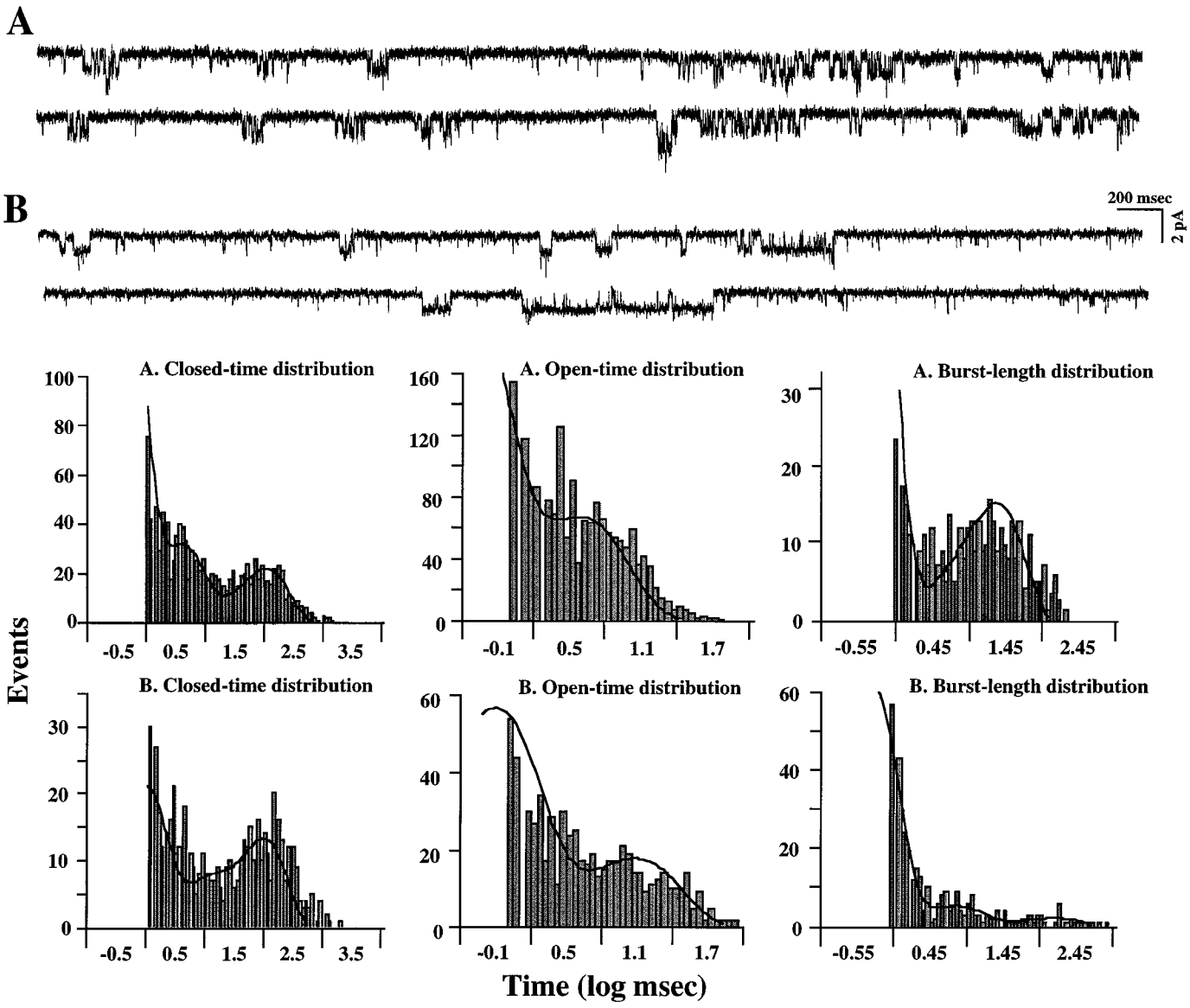

Figure 7. Single-channel activities recorded in the whole-cell configuration. *A, B*, Stretches of single-channel activity recorded in the whole-cell configuration (at 500 Hz bandwidth) in cells clamped at −60 mV in response to 10 μM GABA. Open-time, closed-time, and burst length distributions obtained from the recordings in *A* and *B* are shown in the *bottom panels*. Kinetic analyses were performed on the desensitized state and/or on those stretches of openings with few multiple superimposed events. *A*, The open-time distribution of the channel activity (2144 events) is fitted by two components with τ values of 0.39 ± 0.09 msec (77 ± 9%) and 4.5 ± 0.14 msec (23 ± 1%). The closed-time distribution (1730 events) can be fitted by three components with τ values of 0.28 ± 0.04 msec (80 ± 10%), 3.6 ± 0.08 msec (12 ± 2%), and 107 ± 0.1 msec (8 ± 2%). The burst length distribution (597 events) can be fitted by two components with τ values of 0.89 ± 0.14 (53 ± 20%) and 23.98 ± 0.09 (48 ± 9%). *B*, The open-time distribution (819 events) contains two components with τ values of 0.81 ± 0.16 msec (75 ± 30%) and 12.98 ± 0.30 msec (25 ± 16%). The closed-time distribution (575 events) can be fitted by two components with τ values of 1.15 ± 0.1 msec (58 ± 15%) and 89.2 ± 0.09 msec (42 ± 8%). The burst length distribution (597 events) comprises three components with τ values of 0.29 ± 0.22 msec (91 ± 86%), 4.13 ± 0.42 msec (7 ± 7%), and 108.6 ± 1.1 msec (2 ± 5%).

only activity in response to 2 μM GABA, because it rapidly faded with 10 μM GABA. In contrast, desensitization was slow or absent in slow channels, even when 10 μM GABA was used, and there was no apparent time-dependent drift in the P_{open}. We estimated the number of channels (N) in the cell using three different methods: (1) evaluation of the maximal number of channels observed in the cell, (2) jackknife, and (3) bayesian GC estimator (Horn, 1991). The three methods gave similar results. In some cells, GC gave a slightly higher estimate [$n = 5$ of (1) vs $n = 6$ of (3)]. We used the latter method because (1) is the biased estimate of N. We collected distributions of the dwell times corresponding to different current levels (Figs. 8, 9), which indicated biliganded activation with at least two open and three closed states (Fig. 8*B*). Other nonconducting states connected to the closed-liganded state would prolong the duration of the activated states (Jones and Westbrook, 1996). We found that five closed states and two open states were actually required to fit the spectral properties. To simplify calculations, we did not take into account slowly developing "nonconducting" desensitized states. For each vector of kinetic parameters tested, we calculated the expected probability density functions (pdf) at different current levels. The curves of the pdf fitting distribution histograms were calculated

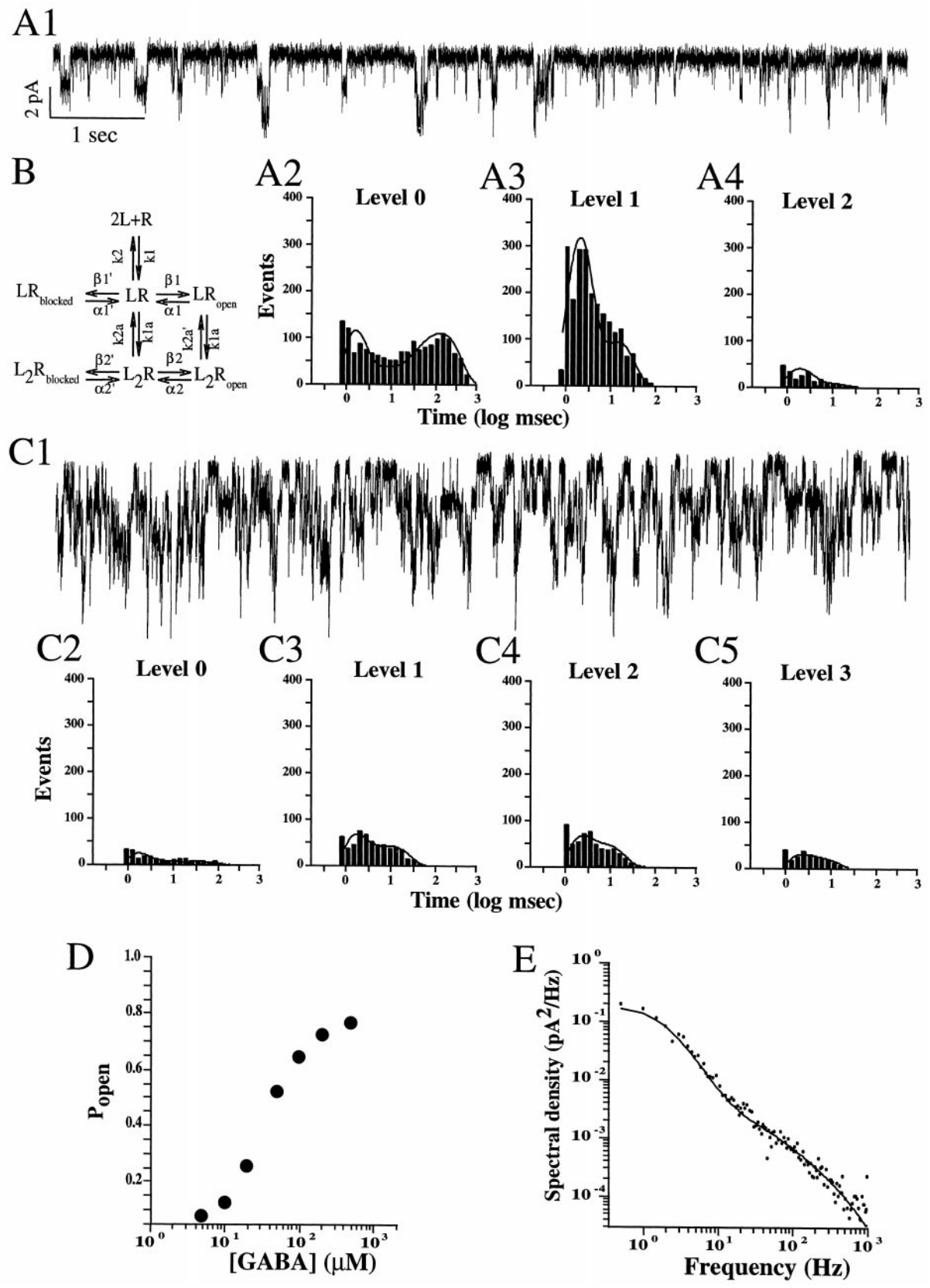

Figure 8. Kinetic analysis of multiple slow channel activities recorded at limited bandwidth. Current activities induced by 2 and 10 μM GABA on the same cell are shown in *A1* and *C1*, respectively. *A1*, 2 μM GABA triggers activity with long closed intervals that are interrupted by many brief openings. Only a few of the openings superimpose. *C1*, 10 μM GABA induces intense activity (5 openings superimpose from time to time), and only short times are spent in the closed state. *B*, Kinetic scheme formulated to calculate theoretical pdf to fit dwell time distributions. *A2–A4*, Dwell time distributions corresponding to level 0 (closed state; *A2*), level 1 (one channel open at a time; *A3*), and level 2 [two channels open at a (*Figure legend continues*)

for the omission of intervals shorter than the dead time (t_d = 0.4 msec). The pdf of an individual channel is a piecewise function of intervals, which are multiples of t_d. The pdf of each interval is the sum of exponentials with coefficients represented by polynomials. The complexity of calculations increases for intervals longer than t_d. For $t \gg t_d$, an approximate solution can be used. To simplify, we have limited the evaluations of the approximate solution to $t \gg t_d$. Therefore, the fitting curve of the estimated pdf is likely to adequately interpolate the dwell time distributions only at time intervals at least three to four times longer than the dead time, and therefore the quickest rate constants may possibly have less accurate estimates. The parameters finally chosen provided a good fit of dwell time distributions in different cells of the same hierarchical cluster (Figs. 8*A2–A4,C2–C5*, 9*A2–A5,B2–B5*). For the fast channels, we estimated $k_1 = 13 \times 10^6\ mol^{-1}\ sec^{-1}$; $k_{1a} = 35 \times 10^6\ mol^{-1}\ sec^{-1}$; $k_2 = 125\ sec^{-1}$; $k_{2a} = 180\ sec^{-1}$; $\beta_1 = 982\ sec^{-1}$; $\alpha_1 = 1080\ sec^{-1}$; $\beta_2 = 725\ sec^{-1}$; $\alpha_2 = 155\ sec^{-1}$; $\beta'_1 = 600\ sec^{-1}$; $\alpha'_1 = 80\ sec^{-1}$; $\beta'_2 = 705\ sec^{-1}$; and $\alpha'_2 = 95\ sec^{-1}$. For the slow channels, we estimated $k_1 = 1.05 \times 10^6\ mol^{-1}\ s^{-1}$; $k_{1a} = 50 \times 10^6\ mol^{-1}\ s^{-1}$; $k_2 = 202\ sec^{-1}$; $k_{2a} = 220\ sec^{-1}$; $\beta_1 = 3480\ sec^{-1}$; $\alpha_1 = 3780\ sec^{-1}$; $\beta_2 = 385\ sec^{-1}$; $\alpha_2 = 46\ sec^{-1}$; $\beta'_1 = 500\ sec^{-1}$; $\alpha'_1 = 33\ sec^{-1}$; $\beta'_2 = 255\ sec^{-1}$; and $\alpha'_2 = 380\ sec^{-1}$. t values of the longest lasting component of the closed-time distribution were sensitive to the number of channels estimated and to the product [GABA] k_1. In contrast, the weight of the latter component was mainly affected by the values of k_2 and k_{2a}. Therefore, the estimated values for these parameters were specifically linked to the features of the observed dwell time distribution. The absence of desensitization with 10 μM GABA in the slow channels allowed us to test the consistency of the estimated values at different concentrations. The latter kinetic parameters predict Lorentzians with corner frequencies of 30 and 1.5 Hz for fast and slow channels, respectively, which for slow channels predict spectra similar to those actually calculated in many recordings. Furthermore, the parameters also account for the relative abundance of power in the 10–50 Hz frequency range characteristic of fast channels, but they do not describe adequately the LF component. The LF component might be explained by the coexistence of slow and fast channels on the same cell or by the clustering of openings between desensitized states of long durations. Finally, estimated kinetic parameters predicted EC_{50} values of ~4 and ~40 μM for the fast and slow channels, respectively, which are consistent with the results. As recently reported (Jones et al., 1998), on-rate binding constants were below the diffusion limits ($10^{-8}\ M^{-1}\ sec^{-1}$).

Interestingly, isomerization rate constants (α and β) were larger than those related to the binding step (k_1, k_2, k_{1a}, and k_{2a}). In a simple kinetic scheme with monoliganded activation, variance analysis underestimates the unitary amplitude by a factor equal to the fraction of time the activated channel is in the open state. In both the slow and fast channels, this value is ~60%. If a similar effect is assumed for the biliganded kinetic scheme, then, for the 27 pS channel, the unitary conductance inferred by variance analysis should be ~18 pS, which is in excellent agreement with the estimates from variance analysis (Table 1).

DISCUSSION

Salient findings

Embryonic hippocampal cells were sorted according to the zolpidem sensitivity of their functional $GABA_A$ receptor/Cl^- channels. Zolpidem-sensitive cells were differentiating neurons, whereas zolpidem-insensitive cells were immature or newly committed neurons. More than 70% of the zolpidem-sensitive neurons expressed α4, α5, β1, β2, β3, γ2, or γ3 subunits, whereas ~50% of the zolpidem-insensitive cells exhibited α4, α5, β1, or γ2 subunits. GABA activated Cl^- ion channels with the same unitary conductance but variable, yet stereotypical patterns of kinetics in both populations. Zolpidem-insensitive cells expressed minimal to moderate numbers of channels whose activation by GABA and modulation by diazepam correlated directly with short- or long-lasting openings. These biophysical and pharmacological properties resemble those reported for specific constructs expressed in recombinant studies. Collectively, the results lead us to conclude that α4, β1, and γ2 subunits may compose short-lasting channels, whereas α5, β1, and γ2 subunits may compose long-lasting channels.

Zolpidem-sorted subpopulations express different $GABA_A$ receptor subunits

Cells from the E19 embryonic hippocampus were sorted according to the sensitivity of their $GABA_A$ receptor/Cl^- channels to zolpidem. The zolpidem-sensitive cells were larger in diameter, process-bearing, nestin$^-$, and TnTx$^+$, indicative of differentiating neurons. The zolpidem-insensitive cells were smaller, spherical, nestin$^+$, and TnTx$^-$, characteristics of undifferentiated cells. TuJ-1 antibody immunostained almost all zolpidem-sensitive cells, confirming their neuronal phenotype (Menezes and Luskin, 1994). Approximately 35% of the zolpidem-insensitive cells were TuJ-1$^+$, half of them costaining with nestin, thus identifying them as newly postmitotic neurons. More cells depolarized to GABA (~60%) than were TuJ-1$^+$ (~35%), indicating that some cells not yet expressing this neuronal epitope already have functional $GABA_A$ receptors, which could modulate proliferation (LoTurco et al., 1995).

Subunit expression patterns among sorted cells differed. Most of the zolpidem-sensitive neurons immunostained with most of the subunit-specific antibodies, indicating the probable coexistence of receptor/channel constructs comprising different subunit combinations in the majority of these neurons. Most of the zolpidem-insensitive cells expressed only α4, α5, β1, and γ2 subunits. These cells exhibited $GABA_A$ receptor/Cl^- channels that were insensitive to zolpidem, despite the putative presence of a functional α5 subunit. It is possible that the absence of other subunits (such as β2, β3, or γ3) accounted for this insensitivity. Our findings are similar to those of Mertens et al. (1993), who showed that zolpidem displayed striking differences in affinity for

←

time; *A4*]. Histograms illustrate the prevalence of the events in levels 0 and 1. *Lines* superimposed on the frequency histograms define the theoretical pdf expected for the rate constants reported in Results. *C2–C5*, Dwell time distributions corresponding to level 0 (closed state; *C2*), level 1 (one channel open at a time; *C3*), level 2 (two channels open at a time; *C4*), and level 3 (three channels open at a time; *C5*). Histograms illustrate the prevalence of events in levels 1–3. *D*, Dose–response plot corresponding to the same kinetic scheme as in *B* and rate constant values fitting the dwell time distributions of *A* and *C*. The model predicts an EC_{50} of ~30–40 mM GABA and maximal P_{open} of ~0.8. The current increase between 10 and 100 μM GABA is approximately sevenfold. *E*, Theoretical spectral density plot expected for scheme *B* and calculated for rate constants fitting dwell time distributions of *A* and *C*. *Dots* correspond to the spectral density derived from actual current fluctuations. The model closely approximates the observed experimental data.

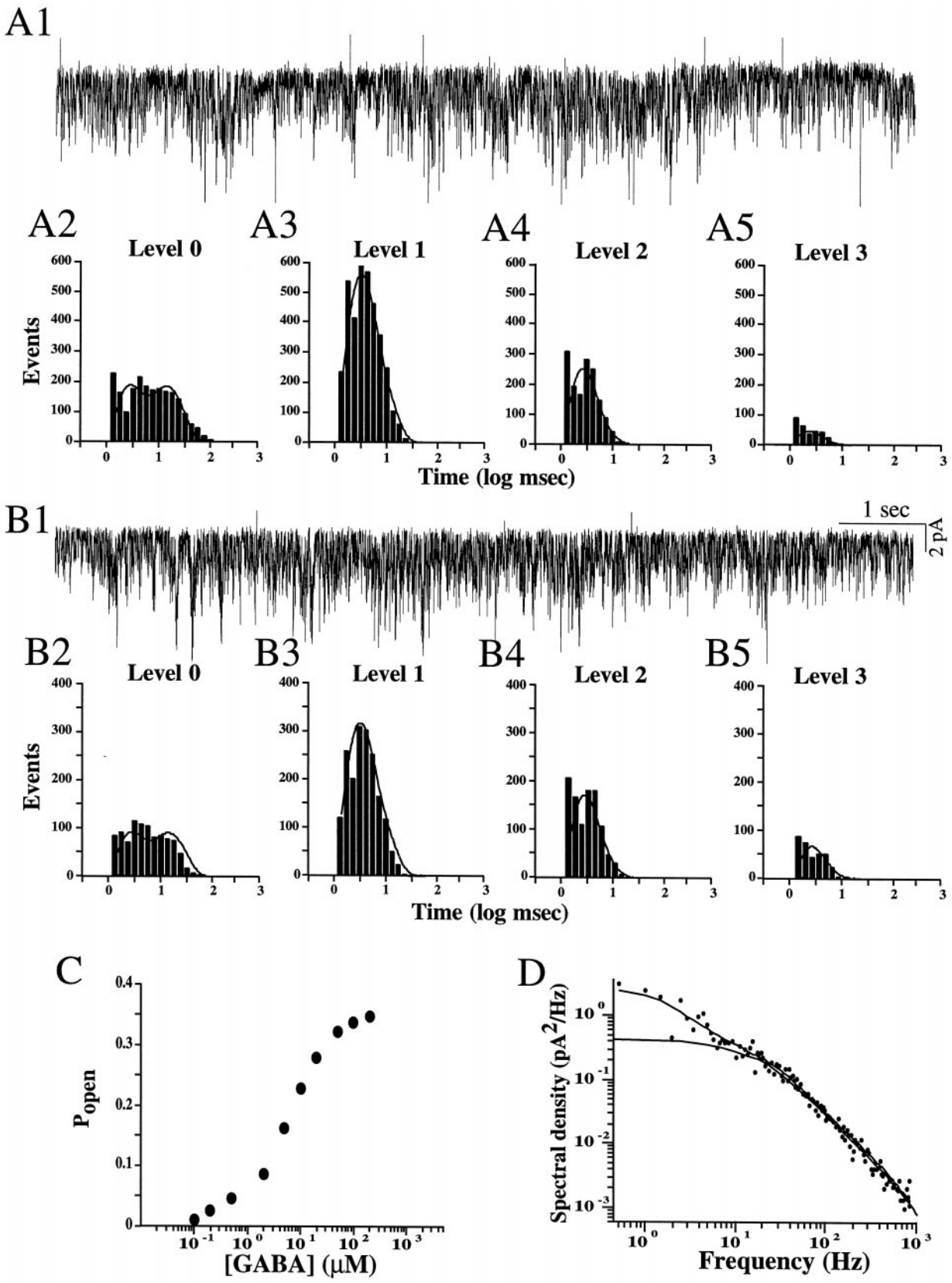

Figure 9. Kinetic analysis of multiple fast channel activities recorded at limited bandwidth. Current activity evoked by 2 mM GABA in two cells is shown in *A1* and *B1*. Both recordings exhibit many characteristic short-lasting openings. *A2–A5, B2–B5*, Dwell time distributions corresponding to level 0 (closed state; *A2*, *B2*), level 1 (one channel open at a time; *A3*, *B3*), level 2 (two channels open at a time; *A4*, *B4*), and level 3 (three channels open at a time; *A5*, *B5*). Histograms illustrate the prevalence of events in the levels 0 and 1. *Lines* superimposed on frequency histograms define the theoretical expected for the rate constants reported in Results. Scheme and rate constants are identical for both recordings. *C*, Dose–response (*Figure legend continues*)

constructs when the $\alpha5$ subunit was coexpressed with different β and γ subunit combinations, indicating a role of other subunits in determining zolpidem affinity.

RT-PCR analysis of sorted subpopulations was in general agreement with the results of immunocytochemical studies, demonstrating marked abundance of $GABA_A$ receptor subunit mRNAs in zolpidem-sensitive neurons compared with zolpidem-insensitive cells. PCR amplification also revealed several subunit transcripts in the zolpidem-insensitive population that were not detected using immunocytochemistry, again suggesting that these cells are more immature, with transcript synthesis preceding expression of the encoded subunit proteins. This was observed as well for $\alpha1$ subunit in the zolpidem-sensitive population, which was expressed at transcript but not protein levels.

Short- and long-lasting channels in zolpidem-insensitive cells may correspond to the expression of $\alpha4\beta1\gamma2$ and $\alpha5\beta1\gamma2$ subunit constructs

Zolpidem-insensitive cells expressed at least two types of channel activity: (1) fast, with short clusters of openings, high affinity for GABA, and modest potentiation by diazepam; and (2) slow, with long clusters of openings, low affinity for GABA, and severalfold potentiation by diazepam. Single-channel activity recorded whole-cell revealed the coexistence of short- and long-lasting openings on the same cell. We have observed a continuity in the distribution of the values of diazepam potentiation, and because there was no evidence for two distinct distributions in the values of diazepam-induced potentiation, different zolpidem-insensitive cells are likely to express variable proportions of constructs with high and low sensitivity to benzodiazepines.

It is possible that fast, short-lasting and slow, long-lasting channels are composed of $\alpha4\beta1\gamma2$ and $\alpha5\beta1\gamma2$ subunit constructs, respectively. The $\alpha5$ subunit is frequently associated with the $\beta1$ subunit in the adult (Laurie et al., 1992). Studies on recombinant receptors indicate that the $\alpha5$-containing constructs have a relatively high EC_{50} for GABA when they are associated with the $\beta1$ subunit (Burgard et al., 1996). The EC_{50} for GABA-gated currents flowing through recombinant $\alpha5\beta1\gamma2$ receptors (36 μM) is close to that estimated for the long-lasting channels observed in the present study. In constructs containing the $\alpha5$ subunit, diazepam has a potentiating effect of 100% (200% of the GABA-activated current in control) (Puia et al., 1991; Burgard et al., 1996), which is in the range of values described in the present study. It has also been demonstrated that the duration of the LF component expressed by embryonic $GABA_A$ receptor/Cl^- channels correlates with the relative expression of the $\alpha5$ mRNA quantified in different regions (Serafini et al., 1998a). Taken together, these properties indicate that long-lasting channels most likely contain $\alpha5\beta1\gamma2$ subunit constructs. Alternatively, these channels might contain $\alpha2$, $\alpha3$, $\beta1$–3, and $\gamma3$ subunits, because these subunits were also immunoidentified. However, with the exception of $\beta1$, these subunits were expressed in <5% of the cells, and thus few cells would be expected to express channels composed of these subunits. Channels containing $\alpha2$ and $\alpha3$ subunits exhibit a significant degree of potentiation by diazepam (Puia et al., 1991), as well as relatively low affinity for GABA (Ebert et al., 1994) and long-lasting open times (Verdoorn, 1994).

Because the other most abundant α subunit in zolpidem-insensitive cells was $\alpha4$, and the constructs containing the $\alpha4$ subunit are expected to be insensitive to either zolpidem (Scholze et al., 1996) or diazepam modulation (Benke et al., 1997), the channels with short-lasting openings, high affinity for GABA, and insensitivity to zolpidem or diazepam might be composed of the $\alpha4\beta1\gamma2$ subunit constructs. $GABA_A$ receptor/Cl^- channels in hippocampal cells sensitive to furosemide (a drug acting on constructs containing $\alpha4$ subunits) have time constants corresponding to those characterized for the short-lasting channels described in the present study (Banks et al., 1998). Recombinant $GABA_A$ receptors expressing the $\gamma2$-subunits are diazepam-insensitive when associated with $\alpha4$ (Benke et al., 1997). Recombinant receptors without any γ subunit have also been reported to have poor sensitivity to zolpidem. However, it is unlikely that receptor constructs without γ subunits were expressed by zolpidem-insensitive cells, because recombinant receptors without γ subunits have a main conductance state of 13 pS (Angelotti and Macdonald, 1993), whereas the main conductance state in our whole-cell recordings of single-channel activity was 27 pS.

Time constant values quantified in the present study may be compared with those previously described for the $GABA_A$/Cl^- channels expressed by hippocampal neurons. Spectral density plots of GABA-evoked Cl^- currents in embryonic hippocampal neurons cultured for ~3–4 weeks were fitted by one component (τ = 23 msec) in an early study by Segal and Barker (1984) and two components with τ values of ~5 and ~51 msec by Ozawa and Yuzaki (1984). Nonstationary fluctuation analysis of IPSCs in the granule cell layer of adult rats showed a spectral density that was fitted by three components with τ values of 25, 1.7, and 0.3 msec, respectively (De Koninck and Mody, 1994). IPSCs recorded in adult rat CA1 neurons were fitted by one exponential with a τ value of either 11 msec (Collingridge et al., 1984) or 25 msec (Ropert et al., 1990). Pearce et al. (1995) have shown that evoked IPSCs were fitted by short (τ = 3–8 msec) or long-lasting exponentials (τ = 30–70 msec), depending on the site of stimulation in CA1. The long-lasting channel durations of ~100 msec recorded in embryonic cells are comparable with the decay of the longest-lasting IPSCs and might correspond to the continued expression of such channels in the adult. Thus, some channels with very-long-lasting openings might contain $\alpha5$, $\beta1$, and $\gamma2$ subunits, both in the embryonic and adult period. This receptor channel type would be of particular pharmacological and clinical relevance, because $\alpha5$ subunit-containing constructs are thought to play roles in epilepsy (Houser et al., 1995) and in tolerance to diazepam (Zhao et al., 1994).

In sum, the advent of functional $GABA_A$ receptor/Cl^- channels among embryonic hippocampal neurons in the earliest stages of differentiation includes assembly of two channel types, with clusters of short- and long-lasting openings of ~30 and ~100 msec, which may be composed of $\alpha4\beta1\gamma2$ and $\alpha5\beta1\gamma2$ subunit constructs, respectively. The long-lasting openings would be ex-

←

plot corresponding to the same kinetic scheme (as in *B*) and rate constant values fitting dwell time distributions of *A* and *B*. The model predicts an EC_{50} of 5 μM GABA and maximal P_{open} of ~0.35. The current increase between 10 and 100 μM is ~40%. *D*, Theoretical spectral density plot (*bottom continuous line*). The *top continuous line* outlines the sum of long- and short-lasting components (290 slow and 950 fast channels). *Dots* correspond to the spectral density derived from actual current fluctuations. The model provides an adequate account for the relative abundance of power in the 10–50 Hz range observed in many spectra. The LF (0.5–10 Hz) component in the spectrum calculated from actual current fluctuations could be explained by the coexistence of the two types of channel kinetics activated in the same cell.

pected to induce significant depolarizing effects, whereas clusters of short-lasting openings would likely be less effective.

REFERENCES

Angelotti TP, Macdonald RL (1993) Assembly of $GABA_A$ receptor subunits: alpha 1 beta 1 and alpha 1 beta 1 gamma 2s subunits produce unique ion channels with dissimilar single-channel properties. J Neurosci 13:1429–1440.

Banks MI, Li TB, Pearce RA (1998) The synaptic basis of $GABA_A$, slow. J Neurosci 18:1305–1317.

Behar TN, Li YX, Tran HT, Ma W, Dunlap V, Scott C, Barker JL (1996) GABA stimulates chemotaxis and chemokinesis of embryonic cortical neurons via calcium-dependent mechanisms. J Neurosci 16:1808–1818.

Benke D, Cicin-Sain A, Mertens S, Mohler H (1991) Immunochemical identification of the alpha 1- and alpha 3-subunits of the $GABA_A$-receptor in rat brain. J Recept Res 11:407–424.

Benke D, Fritschy JM, Trzeciak A, Bannwarth W, Mohler H (1994) Distribution, prevalence, and drug binding profile of gamma-aminobutyric acid type A receptor subtypes differing in the beta-subunit variant. J Biol Chem 269:27100–27107.

Benke D, Michel C, Mohler H (1997) GABA(A) receptors containing the alpha4-subunit: prevalence, distribution, pharmacology, and subunit architecture in situ. J Neurochem 69:806–814.

Buchstaller A, Fuchs K, Sieghart W (1991) Identification of alpha 1-, alpha 2- and alpha 3-subunit isoforms of the $GABA_A$-benzodiazepine receptor in the rat brain. Neurosci Lett 129:237–241.

Burgard EC, Tietz EI, Neelands TR, Macdonald RL (1996) Properties of recombinant gamma-aminobutyric acid A receptor isoforms containing the alpha 5 subunit subtype. Mol Pharmacol 50:119–127.

Collingridge GL, Gage PW, Robertson B (1984) Inhibitory post-synaptic currents in rat hippocampal CA1 neurones. J Physiol (Lond) 356:551–564.

Colquhoun D, Hawkes AG (1977) Relaxation and fluctuations of membrane currents that flow through drug- operated channels. Proc R Soc Lond B Biol Sci 199:231–262.

De Koninck Y, Mody I (1994) Noise analysis of miniature IPSCs in adult rat brain slices: properties and modulation of synaptic $GABA_A$ receptor channels. J Neurophysiol 71:1318–1335.

Ebert B, Wafford KA, Whiting PJ, Krogsgaard-Larsen P, Kemp JA (1994) Molecular pharmacology of gamma-aminobutyric acid type A receptor agonists and partial agonists in oocytes injected with different alpha, beta, and gamma receptor subunit combinations. Mol Pharmacol 46:957–963.

Hawkes AG, Jalali A, Colquhoun D (1992) Asymptotic distributions of apparent open times and shut times in a single channel record allowing for the omission of brief events. Philos Trans R Soc Lond B Biol Sci 337:383–404.

Hockfield S, McKay RD (1985) Identification of major cell classes in the developing mammalian nervous system. J Neurosci 5:3310–3328.

Horn R (1991) Estimating the number of channels in patch recordings. Biophys J 60:433–439.

Houser CR, Esclapez M, Fritschy JM, Mohler H (1995) Decreased expression of the $\alpha 5$ subunit of the $GABA_A$ receptor in a model of temporal lobe epilepsy. Soc Neurosci Abstr 2:1475.

Jones MV, Westbrook GL (1996) The impact of receptor desensitization on fast synaptic transmission. Trends Neurosci 19:96–101.

Jones MV, Sahare Y, Dzubay JA, Westbrook GL (1998) Defining affinity with the $GABA_A$ receptor. J Neurosci 18:8550–8604.

Kijima S, Kijima H (1987) Statistical analysis of channel current from a membrane patch. II. A stochastic theory of a multi-channel system in the steady-state. J Theor Biol 128:435–455.

Koulakoff A, Bizzini B, Berwald-Netter Y (1983) Neuronal acquisition of tetanus toxin binding sites: relationship with the last mitotic cycle. Dev Biol 100:350–357.

Kristiansen U, Barker JL, Serafini R (1995) The low efficacy gamma-aminobutyric acid type A agonist 5-(4-piperidyl)isoxazol-3-ol opens brief Cl^- channels in embryonic rat olfactory bulb neurons. Mol Pharmacol 48:268–279.

Laurie DJ, Wisden W, Seeburg PH (1992) The distribution of thirteen $GABA_A$ receptor subunit mRNAs in the rat brain. III. Embryonic and postnatal development. J Neurosci 12:4151–4172.

Lee MK, Tuttle JB, Rebhun LI, Cleveland DW, Frankfurter A (1990) The expression and posttranslational modification of a neuron-specific beta-tubulin isotype during chick embryogenesis. Cell Motil Cytoskeleton 17:118–132.

LoTurco JJ, Owens DF, Heath MJ, Davis MB, Kriegstein AR (1995) GABA and glutamate depolarize cortical progenitor cells and inhibit DNA synthesis. Neuron 15:1287–1298.

Ma W, Barker JL (1995) Complementary expressions of transcripts encoding GAD67 and $GABA_A$ receptor alpha 4, beta 1, and gamma 1 subunits in the proliferative zone of the embryonic rat central nervous system. J Neurosci 15:2547–2560.

Ma W, Saunders PA, Somogyi R, Poulter MO, Barker JL (1993) Ontogeny of $GABA_A$ receptor subunit mRNAs in rat spinal cord and dorsal root ganglia. J Comp Neurol 338:337–359.

Maric D, Maric I, Ma W, Lahjouji F, Somogyi R, Wen X, Sieghart W, Fritschy J-M, Barker JL (1997) Anatomical gradients in proliferation and differentiation of embryonic rat CNS accessed by buoyant density fractionation: $\alpha 3$, $\beta 3$ and $\gamma 2$ $GABA_A$ receptor subunit co-expression by post-mitotic neocortical neurons correlates directly with cell buoyancy. Eur J Neurosci 9:507–522.

Maric D, Maric I, Smith SV, Serafini R, Hu Q, Barker JL (1998) Potentiometric study of resting potential, contributing K^+ channels and the onset of Na^+ channel excitability in embryonic rat cortical cells. Eur J Neurosci 10:2532–2546.

Marksitzer R, Benke D, Fritschy JM, Trzeciak A, Bannwarth W, Mohler H (1993) $GABA_A$-receptors: drug binding profile and distribution of receptors containing the alpha 2-subunit in situ. J Recept Res 13:467–477.

McKernan RM, Quirk K, Prince R, Cox PA, Gillard NP, Ragan CI, Whiting P (1991) $GABA_A$ receptor subtypes immunopurified from rat brain with alpha subunit-specific antibodies have unique pharmacological properties. Neuron 7:667–676.

Menezes JR, Luskin MB (1994) Expression of neuron-specific tubulin defines a novel population in the proliferative layers of the developing telencephalon. J Neurosci 14:5399–5416.

Mertens S, Benke D, Mohler H (1993) $GABA_A$ receptor populations with novel subunit combinations and drug binding profiles identified in brain by alpha 5- and delta-subunit-specific immunopurification. J Biol Chem 268:5965–5973.

Mienville JM, Lange GD, Barker JL (1994) Reciprocal expression of cell-cell coupling and voltage-dependent Na current during embryogenesis of rat telencephalon. Brain Res Dev Brain Res 77:89–95.

Mossier B, Togel M, Fuchs K, Sieghart W (1994) Immunoaffinity purification of gamma-aminobutyric acid A ($GABA_A$) receptors containing gamma 1-subunits. Evidence for the presence of a single type of gamma-subunit in $GABA_A$ receptors. J Biol Chem 269:25777–25782.

Owens DF, Boyce LH, Davis MB, Kriegstein AR (1996) Excitatory GABA responses in embryonic and neonatal cortical slices demonstrated by gramicidin perforated-patch recordings and calcium imaging. J Neurosci 16:6414–6423.

Ozawa S, Yuzaki M (1984) Patch-clamp studies of chloride channels activated by gamma- aminobutyric acid in cultured hippocampal neurones of the rat. Neurosci Res 1:275–293.

Paxinos G, Tork I, Tecott LH, Valentino KL (1991) Developing rat brain. San Diego: Academic.

Pearce RA, Grunder SD, Faucher LD (1995) Different mechanisms for use-dependent depression of two $GABA_A$-mediated IPSCs in rat hippocampus. J Physiol (Lond) 484:425–435.

Poulter MO, Barker JL, O'Carroll AM, Lolait SJ, Mahan LC (1992) Differential and transient expression of $GABA_A$ receptor alpha-subunit mRNAs in the developing rat CNS. J Neurosci 12:2888–2900.

Puia G, Vicini S, Seeburg PH, Costa E (1991) Influence of recombinant gamma-aminobutyric acid-A receptor subunit composition on the action of allosteric modulators of gamma- aminobutyric acid-gated Cl^- currents. Mol Pharmacol 39:691–696.

Ropert N, Miles R, Korn H (1990) Characteristics of miniature inhibitory postsynaptic currents in CA1 pyramidal neurones of rat hippocampus. J Physiol (Lond) 428:707–722.

Ruano D, Vizuete M, Cano J, Machado A, Vitorica J (1992) Heterogeneity in the allosteric interaction between the gamma-aminobutyric acid (GABA) binding site and three different benzodiazepine binding sites of the $GABA_A$/benzodiazepine receptor complex in the rat nervous system. J Neurochem 58:485–493.

Sanger DJ, Benavides J, Perrault G, Morel E, Cohen C, Joly D, Zivkovic B (1994) Recent developments in the behavioral pharmacology of benzodiazepine (omega) receptors: evidence for the functional significance of receptor subtypes. Neurosci Biobehav Rev 18:355–372.

Scholze P, Ebert V, Sieghart W (1996) Affinity of various ligands for-$GABA_A$ receptors containing alpha 4 beta 3 gamma 2, alpha 4 gamma 2, or alpha 1 beta 3 gamma 2 subunits. Eur J Pharmacol 304:155–162.

Segal M, Barker JL (1984) Rat hippocampal neurons in culture: properties of GABA-activated Cl^- ion conductance. J Neurophysiol 51:500–515.

Serafini R, Valeyev AY, Barker JL, Poulter MO (1995) Depolarizing GABA-activated Cl^- channels in embryonic rat spinal and olfactory bulb cells. J Physiol (Lond) 488:371–386.

Serafini R, Maric I, Wen XL, Somogyi R, Barker JL, Maric D (1996) Subunit composition and functional properties of zolpidem-insensitive $GABA_A$ receptor channels of embryonic rat hippocampal cells. Soc Neurosci Abstr 1:811.

Serafini R, Maric D, Maric I, Ma W, Fritschy JM, Zhang L, Barker JL (1998a) Dominant GABA(A) receptor/Cl^- channel kinetics correlate with the relative expressions of alpha2, alpha3, alpha5 and beta3 subunits in embryonic rat neurones. Eur J Neurosci 10:334–349.

Serafini R, Ma W, Maric D, Maric I, Lahjouji F, Sieghart W, Barker JL (1998b) Initially expressed early rat embryonic GABA(A) receptor Cl^- ion channels exhibit heterogeneous channel properties. Eur J Neurosci 10:1771–1783.

Somogyi R, Wen X, Ma W, Barker JL (1995) Developmental kinetics of GAD family mRNAs parallel neurogenesis in the rat spinal cord. J Neurosci 15:2575–2591.

Sperk G, Schwarzer C, Tsunashima K, Fuchs K, Sieghart W (1997) GABA(A) receptor subunits in the rat hippocampus I: immunocytochemical distribution of 13 subunits. Neuroscience 80:987–1000.

Todd AJ, Watt C, Spike RC, Sieghart W (1996) Colocalization of GABA, glycine, and their receptors at synapses in the rat spinal cord. J Neurosci 16:974–982.

Verdoorn TA (1994) Formation of heteromeric gamma-aminobutyric acid type A receptors containing two different alpha subunits. Mol Pharmacol 45:475–480.

Zhao TJ, Chiu TH, Rosenberg HC (1994) Reduced expression of gamma-aminobutyric acid type A/benzodiazepine receptor gamma 2 and alpha 5 subunit mRNAs in brain regions of flurazepam-treated rats. Mol Pharmacol 45:657–663.